

UNIDIRECTIONAL SOLIDIFICATION OF RARE EARTH OXIDE-METAL COMPOSITES

A THESIS

Presented to

The Faculty of the Graduate Division

by

James Windsor Stendera

In Partial Fulfillment

of the Requirements for the Degree


Master of Science in Ceramic Engineering

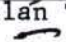
Georgia Institute of Technology


September, 1974

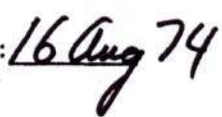
UNIDIRECTIONAL SOLIDIFICATION OF RARE EARTH
OXIDE-METAL COMPOSITES

A _____ 7

 James F. Benzel, Chairman

 Alan T. Chapman

 Robert K. Feene

Date Approved by Chairman: 

ACKNOWLEDGEMENTS

"Ask, and it shall be given; seek and ye shall find; knock and it shall be opened unto you: for everyone that asketh receiveth; and he that seeketh findeth; and to him that knocketh; it shall be opened."

Matthew 7:7

The author wishes to thank all those people who, in ways large and small, assisted me in completing this project. Special thanks goes to Dr. A. T. Chapman, Dr. J. F. Benzel, and Dr. R. K. Feeney, who served on the reading committee and whose help transformed my efforts into readable English.

TABLE OF CONTENTS

| | Page |
|---|------|
| ACKNOWLEDGEMENTS | ii |
| LIST OF TABLES | v |
| LIST OF ILLUSTRATIONS | vi |
| SUMMARY | ix |
| Chapter | |
| I. INTRODUCTION | 1 |
| II. SURVEY | 3 |
| RF Heating and Its Use in Ceramic Melting Applications | |
| Oxide Metal Composites | |
| UO ₂ | |
| ZrO ₂ Stabilized with CaO or Y ₂ O ₃ | |
| HfO ₂ Stabilized with Y ₂ O ₃ | |
| MgO and Cr ₂ O ₃ | |
| Summary | |
| Metal-Metal Solidification | |
| Rod-Malellar | |
| Cellular Growth | |
| Banding | |
| Coupled Zone | |
| Rare Earth Oxides | |
| III. EQUIPMENT. | 31 |
| Induction Heating Unit | |
| Growth Apparatus | |
| IV. GROWTH PROCEDURE | 35 |
| Pellet Preparation | |
| Growth Procedure | |
| Examination | |

TABLE OF CONTENTS (Continued)

| | Page |
|--|------|
| V. DISCUSSION AND RESULTS | 41 |
| Composite Growth in the Rare-Earth Oxide Metal Systems | |
| Effect of CeO ₂ Additions | |
| Metal Content and Growth Rate | |
| Metal Morphology | |
| Banding | |
| Chemical Etching | |
| VI. CONCLUSIONS | |
| VII. BIBLIOGRAPHY | |

LIST OF TABLES

| Table | Page |
|---|------|
| 1. Summary of Composite Growth in the Rare Earth Oxide-Metal Systems | 43 |
| 2. Summary of the Solidification of Excess Metal Samples Grown at Fast Rates to Test the Coupled Growth Theory | 59 |
| 3. Summary of Attempts to Artificially Induce Interrupted (Banded) Fiber Growth in Nd_2O_3 - CeO_2 -Mo Samples | 72 |

LIST OF ILLUSTRATIONS

| Figure | Page |
|--|------|
| 1. Power Absorbed as a Function of the Radius-to-Skin Depth Ratio | 5 |
| 2. Proposed UO_2 -W Phase Diagram | 11 |
| 3. Fiber Diameter and Density vs Growth Rate in the Systems UO_2 -W and ZrO_2 -W | 12 |
| 4. Nucleation of a Eutectic Grain | 17 |
| 5. Idealized Lamellar Shape and Factors Governing Growth | 19 |
| 6. Conventional Phase Diagrams Showing the Coupled Region | 27 |
| 7. Phase Transformations of the Rare Earth Sesquioxides. | 29 |
| 8. Equilibrium Oxygen Partial Pressure as a Function of Ceria Composition | 30 |
| 9. Induction Heating Facilities | 33 |
| 10. Schematic Diagram of the Induction Heating Facilities | 34 |
| 11. Macroscopic View of Two Gd_2O_3 - CeO_2 -Mo Samples Which Have Been Longitudinally Sectioned After Growth | 45 |
| 12. Transverse and Longitudinal Sections of "good" Fiber Growth in the System Gd_2O_3 - CeO_2 -Mo. | 46 |
| 13. Transverse Section of a Er_2O_3 - CeO_2 -Mo Sample Showing A Distinct Boundary | 47 |
| 14. Longitudinal Sections Comparing Fiber Growth in Nd_2O_3 -Mo Samples with and Without CeO_2 Additions | 50 |
| 15. Increase in CO Lattice Parameter of Nd_2O_3 as a Function of CeO_2 Additions | 51 |
| 16. Transverse Microstructure of a Gd_2O_3 - CeO_2 -Mo Sample Through Which the Molten Zone was Passed Twice | 53 |

LIST OF ILLUSTRATION (continued)

| Figure | Page |
|--|------|
| 17. Longitudinal Section of a Gd_2O_3 - CeO_2 -Mo Sample With a High Starting Metal Content | 54 |
| 18. Transverse Section of a Gd_2O_3 - CeO_2 -Mo Sample with a Low Starting Metal Content | 55 |
| 19. Proposed Gd_2O_3 -20 w/o CeO_2 -Mo Phase Diagram | 57 |
| 20. Typical Gd_2O_3 - CeO_2 -Mo Samples Cut Parallel to the Growth Direction Showing the Effect of Different Growth Rates on Fiber Structure | 60 |
| 21. Effect of Growth Rate on Fiber Density in the System Gd_2O_3 -20 w/o CeO_2 -Mo | 62 |
| 22. Transverse Sections of Nd_2O_3 - CeO_2 -Mo Samples Displaying Three Types of Mo Morphology | 63 |
| 23. Transverse Sections of 20 wt% CeO_2 Doped Nd_2O_3 -Mo Showing the Transition from Fiber to Platelet Morphology from Base to Top of the Solidified Zone. | 64 |
| 24. CeO_2 Doped Gd_2O_3 -Mo Sample Grown at 4 cm/hr displaying Mo Fibers in the Cell Interior which Gradually Change to Platelets as the Cell Boundary is Approached | 66 |
| 25. CeO_2 Doped Gd_2O_3 -Mo Sample Grown at 2 cm/hr Showing Cell Essentially Composed of Narrow Mo Platelets | 67 |
| 26. Schematic Diagram Showing How a Lead by the Metal Phase Might Allow the Metal to Grow in a Secondary Direction and Form Platelets | 68 |
| 27. High Magnification View of a Band Induced Through Power Fluctuation | 70 |
| 28. Longitudinal Section of a Nd_2O_3 - CeO_2 -Mo Sample Showing Two Narrow Bands of Pure Oxide | 71 |
| 29. Longitudinally Sectioned Molten Zone of a Nd_2O_3 - CeO_2 -Mo Sample Showing Regularly Spaced Bands Induced Through Power Fluctuation | 73 |

LIST OF ILLUSTRATIONS (Continued)

| Figure | Page |
|---|------|
| 30. Scanning Electron Micrograph Showing the Selective Etching of the Mo Fibers Leaving an Array of Holes in the Oxide Matrix | 76 |
| 31. SEM Photographs Showing the Improvement in Etching Uniformity Resulting from Annealing | 78 |
| 32. SEM Photographs of a Series of Samples Etched with NH_4NO_3 in Sulfuric Acid | 79 |

SUMMARY

The internal molten zone technique was used to unidirectionally solidify a variety of rare earth oxide-metal compositions. Structures containing from 8 to 50×10^6 , less than $1 \mu\text{m}$ metal fibers/cm² in a ceramic matrix were obtained. It was found that CeO₂ additions to the sesquioxides were necessary for uniform fiber growth. The systems Nd₂O₃-CeO₂-Mo and Gd₂O₃-CeO₂-Mo were investigated in detail in order to characterize rare earth oxide-metal composites. Various chemical etching techniques were developed in order to produce various fiber-matrix geometries.

CHAPTER I

INTRODUCTION

Several methods have been used to unidirectionally solidify oxide-metal mixtures to produce composites with an ordered microstructure composed of submicron metal rods or platelets in an oxide matrix. To date the largest and most uniform oxide-metal composites reported have been grown using the direct rf coupling floating internal molten zone technique. The main advantage of this technique is that the molten zone is self contained by the unmelted skin which eliminates the containment and contamination problems inherent in other methods. Its major disadvantages include (a) limited sample size, (b) limited sample materials, because only a few refractory oxides possess sufficient high temperature electrical conductivity to support eddy current heating and high enough melting points to allow radiation cooling of the skin, and (c) chemical stability to avoid major stoichiometry changes during melting.

Prior to this investigation ordered oxide-metal structures had been achieved using the direct rf coupling technique in the UO_2 -metal (Ta or W) stabilized ZrO_2 -W, and stabilized HfO_2 -W systems. These systems show major drawbacks, however. It is impossible in the hafnia and zirconia systems to produce crack-free samples even with proper stabilization, and in the UO_2 systems oxide stoichiometry is very critical and must be precisely controlled to obtain good growth. Due to these

problems considerable effort was expended to find other oxide metal systems suitable for the direct rf coupling technique.

The high melting points and stoichiometric stability of the rare earth oxides suggested their possible use as composite matrix materials. The purpose of this study was to investigate the suitability of the rare earth oxides for the direct rf coupling technique, and to characterize the parameters affecting the growth of rare earth oxide-metal composites. Not only did the results of this study enable uniform rare earth oxide-metal composites to be routinely grown but also a clearer understanding of the growth processes of all oxide-metal composites was gained.

CHAPTER II

SURVEY

In this section a literature review relating to the subject of unidirectional solidification of rare earth oxide-metal composites is presented. It includes a discussion of rf heating and its use in ceramic melting applications, a brief review of the oxide-metal systems previously unidirectionally solidified, a discussion of findings in metal-metal solidification which relate to oxide-metal solidification, and a short section giving background information on rare earth oxides.

RF Heating and Its Use in Ceramic Melting Applications

Tudbury¹ states that induction heating occurs when an electrically conducting object is placed in a time varying magnetic field. The time varying magnetic field is usually produced by passing alternating current through a coil around the conductor or workpiece to be heated. The magnetic field thus produced induces eddy currents in the workpiece which cause resistance (I^2R) heating. The power absorbed by a solid cylinder in an rf field is related to A^* or the ratio of workpiece radius to reference depth where:

$$A^* = r/d \quad (1)$$

and r = radius of the workpiece

d = reference depth.

The reference depth is defined as the distance below the surface of the conductor that the current density is reduced to $1/e$ or approximately 37 percent of the surface density. The value of the reference depth is given by Equation 2.

$$d = (\pi \cdot \mu \cdot f \cdot \epsilon)^{-\frac{1}{2}} \quad (2)$$

where ϵ = the resistivity

μ = the relative magnetic permeability

f = the frequency

From these relationships it is possible to determine the power absorbed by the workpiece as a function of A^* as shown in Figure 1. It is obvious that a value of A^* of two or three is desirable, but much lower values are acceptable if sufficient power is available.

Induction heating has long been used in industrial metal heating applications especially in forging, heat treating, and foundry operations. Leatherman and Stutz² gave the following advantages of induction heating:

1. No contact between the heat source and the workpiece.
2. High temperatures are attainable.
3. Heating is rapid.
4. Heat can be restricted to localized areas.
5. Controlled atmospheres can be easily used.

These advantages make induction heating very attractive in oxide heating and melting operations. Unfortunately, the high resistivities of the oxides make the values of " d " very large, which make the values of A^* very small. If the frequency could be raised sufficiently,

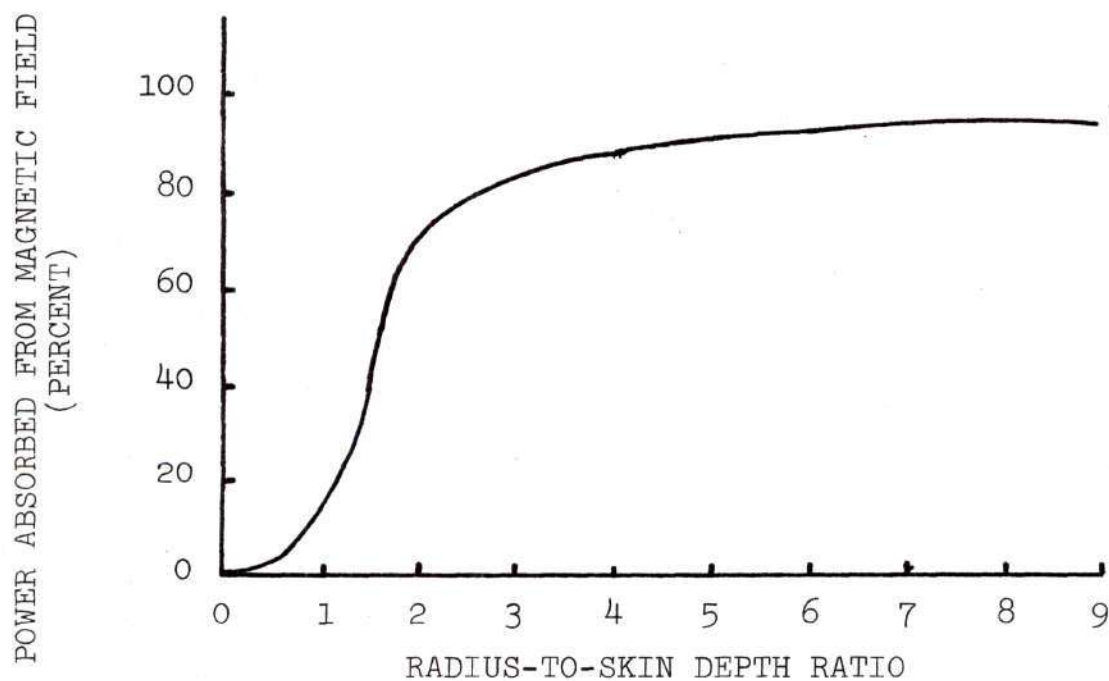


Figure 1. Power Absorbed by a Conductor in a Magnetic Field as a Function the Radius-to-Skin Depth Ratio.

the values of "d" could be made acceptable, but the practical limit to frequency is about 30 MHz. Above this value, current is very difficult to contain on a copper tube, and turn to turn and workpiece to coil arcing becomes a problem. Even at 30 MHz "d" is still too low to permit heating of an insulator unless enormous power is expended. Unlike metals, however, oxide conductance increases with temperature. Therefore, if the sample is preheated before being exposed to the rf field it is possible that the conductance will be raised high enough so that A^* will become large enough for efficient rf heating.

Due to its versatility rf heating has seen wide use in ceramic melting and crystal growing techniques. Usually a metal or carbon crucible is used for containment and as a susceptor. Viechnicki and Schmid³ have described how rf heating was used to unidirectionally solidify an $\text{Al}_2\text{O}_3\text{-Y}_3\text{Al}_5\text{O}_{12}$ eutectic in W crucibles heated by a 450 KHz 20 KW rf generator. A major drawback to the use of a crucible is that it often contaminates the sample making the results unreliable. It is desirable to use the material itself as the susceptor and crucible. This can be easily accomplished with carbides since these materials possess sufficient conductivity at room temperature for induction heating, and the surface tension of the liquid is high enough to maintain a stable zone. Haggerty, Lee and Wencus⁴, using a 10 KW 450 KHz rf generator grew various carbide and boride single crystals by melting the tip of a poly crystalline rod, lowering it onto a seed crystal and slowly lowering both seed and feed rod through the coil.

As mentioned earlier most stoichiometric oxides do not possess sufficient conductivity at room temperature to support induction heating; however, several schemes have been advanced whereby oxide melts can be initiated and maintained with induction heating.

Holt⁵ found that titania could be directly induction heated from room temperature if the oxide was first reduced. He produced TiO_2 single crystals by initiating a melt on a feed rod, lowering the rod until it touched a seed crystal then lowering the rod and seed through a coil, thus passing the molten zone through the feed rod. Holt noted that surface tension was low, but it was enough to hold the melt between the feed rod and grown crystal rod.

Nestor⁶ employed a molten pool of oxide that was initiated by packing the powdered oxide, to be melted, around a graphite susceptor inside an induction coil. The graphite was easily heated until the surrounding oxide has been melted. Once the oxide was molten, it possessed sufficient conductivity to directly couple to the rf field, and the susceptor was removed. Barium zirconate, strontium titanate, zirconia, barium titanate, and alumina single crystals were pulled using the Czochralski technique⁶ from molten pools initiated by the above technique and sustained by rf heating.

Certain stoichiometrically stable refractory oxides can also be directly induction melted by preheating to raise their conductivity with a metal susceptor before exposing the pellet directly to the rf field. Once direct coupling has been established, an internal molten zone is formed with a solid outer skin. The high radiant heat loss from the surface and the low thermal conductivity of the oxides maintains the skin below the melting point.

Chapman and Clark⁷ grew UO_2 single crystals by preheating to 1500°C before exposing the pellet to the rf field, which produced an internal molten zone. The zone was then passed through the pellet by slowly lowering the pellet through the coil. Molybdenum pre and post-heaters were used to reduce thermal gradients along the rod during growth. Spinning the sample during growth was necessary to avoid cellular grain growth, and produce a single crystal. They speculated that centrifugal forces redistributed the liquid so that the growth front was convex and the leading growth occurred along the rod axis, thus favoring single crystal growth.

Hill⁸ initiated internal molten zones in CeO_2 , TiO_2 , CaO stabilized ZrO_2 , Cr_2O_3 , and BaTiO_3 pellets by preheating them to 1500°C before exposing the pellets to rf fields of from 6-30 MHz. He observed stoichiometry changes upon melting in all of the oxides except CaO stabilized ZrO_2 . Chapman et al.⁹ expanded Hill's work and tested a number of oxides and oxide mixtures at various rf frequencies and preheat temperatures to determine if a stable molten zone could be established. A stable molten zone was established in CaO stabilized HfO_2 , however, stable zones could not be established in the other systems for the following reasons:

1. Coupling efficiency was too low to provide the power necessary to achieve an internal molten zone.
2. Surface of the pellets did not emit enough thermal energy to remain solid and contain the liquid.
3. The specimens cracked due to thermal stresses.

4. The starting materials were unstable due to sublimation or stoichiometric changes.

Oxide Metal Composites

Chapman et al.¹⁰, using a technique similar to the one used to produce UO_2 single crystals, grew UO_2 -W cermets. Since that time a number of other oxide-metal systems have been successfully unidirectionally solidified to produce ordered microstructures. A review of this work is presented in this section which is subdivided according to the oxide matrix.

UO_2

Chapman et al.^{9,11} grew UO_2 -W composites using the direct rf coupling internal floating zone technique. In this technique pressed rods of the oxide-metal mixture were sintered inside rf heated Mo tubes in an inert atmosphere. After the initial heating which not only sintered, but preheated the rod, the Mo tube heaters were separated to expose about 2 cm of the rod to an rf field of 3 to 30 MHz. The concurrent increase in temperature, electrical conductivity, and resistance heating continued until the interior of the rod melted. The high radiant heat loss and low thermal conductivity of the rod maintained a solid outer skin. Composite growth was obtained by moving the molten zone through the rod. Two structures were observed, the first type was composed essentially of W fibers uniformly distributed across the melted zone interrupted only by cell or colony boundaries, while the second type had circular areas of oxide bounded by composite structure. They proposed a phase diagram

(see Figure 2) and explained that the first type of structure was at or near the eutectic composition while the second type was on the oxide rich side. The primary phase nucleated at a temperature higher than the eutectic temperature and as cooling proceeded the composition of the remaining liquid moved down the liquidus line until the composition of the eutectic was reached, at which point eutectic solidification began. They also observed that as the growth rate was increased the composition of the eutectic structure became richer in W. They theorized that as growth rate increased, supercooling increased and the composition of the liquid followed the metastable extension of the liquidus line. It was found that fiber diameter varied inversely, and fiber density directly, with increasing growth rate as seen in Figure 3. Oxygen potential in the growth atmosphere and starting stoichiometry were found to be critically important in controlling metal solubility and the resultant composite structure. Although the metal fiber morphology most often seen were circular rods, platelets were occasionally observed.

Jen¹² attempted to grow UO_2 -metal composites using Ta, Nb, or Mo as the metal. Only isolated fiber areas were observed in the UO_2 -Mo system which was blamed on poor metal solubility in the molten oxide. No fibers were observed in the system UO_2 -Nb which was attributed to the high vapor pressure of Nb at UO_2 melting temperatures. Extensive fiber growth was obtained in the UO_2 -Ta system. Fiber areas contained from 12 to 14 wt % Ta and for growth rates of 1.7 cm/hr there were about 1.3×10^7 fibers/cm². A starting oxide stoichiometry of $\text{UO}_{2.03}$ was found to be necessary for good composite

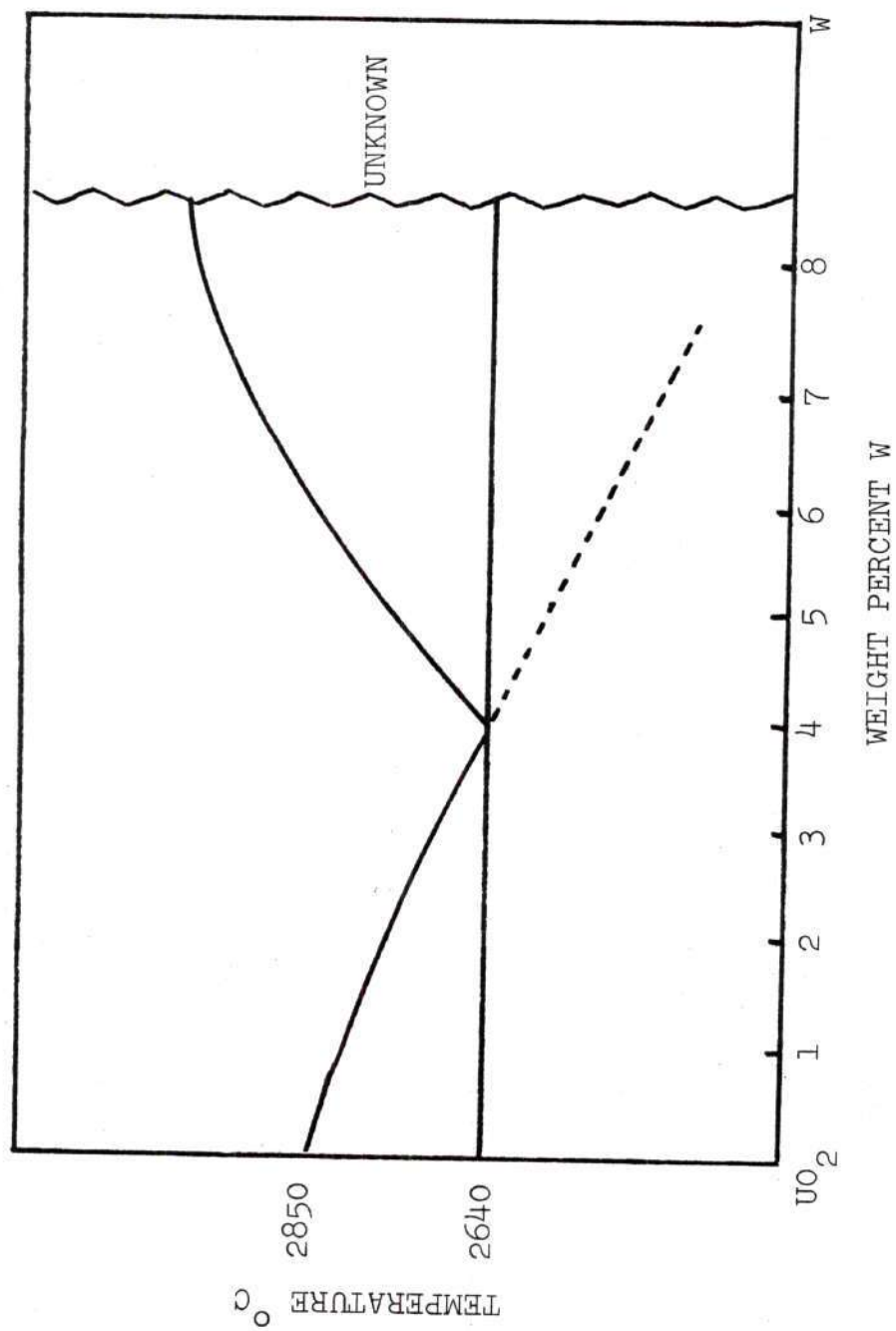


Figure 2. Proposed UO_2 -W Phase Diagram, (After Chapman¹¹).

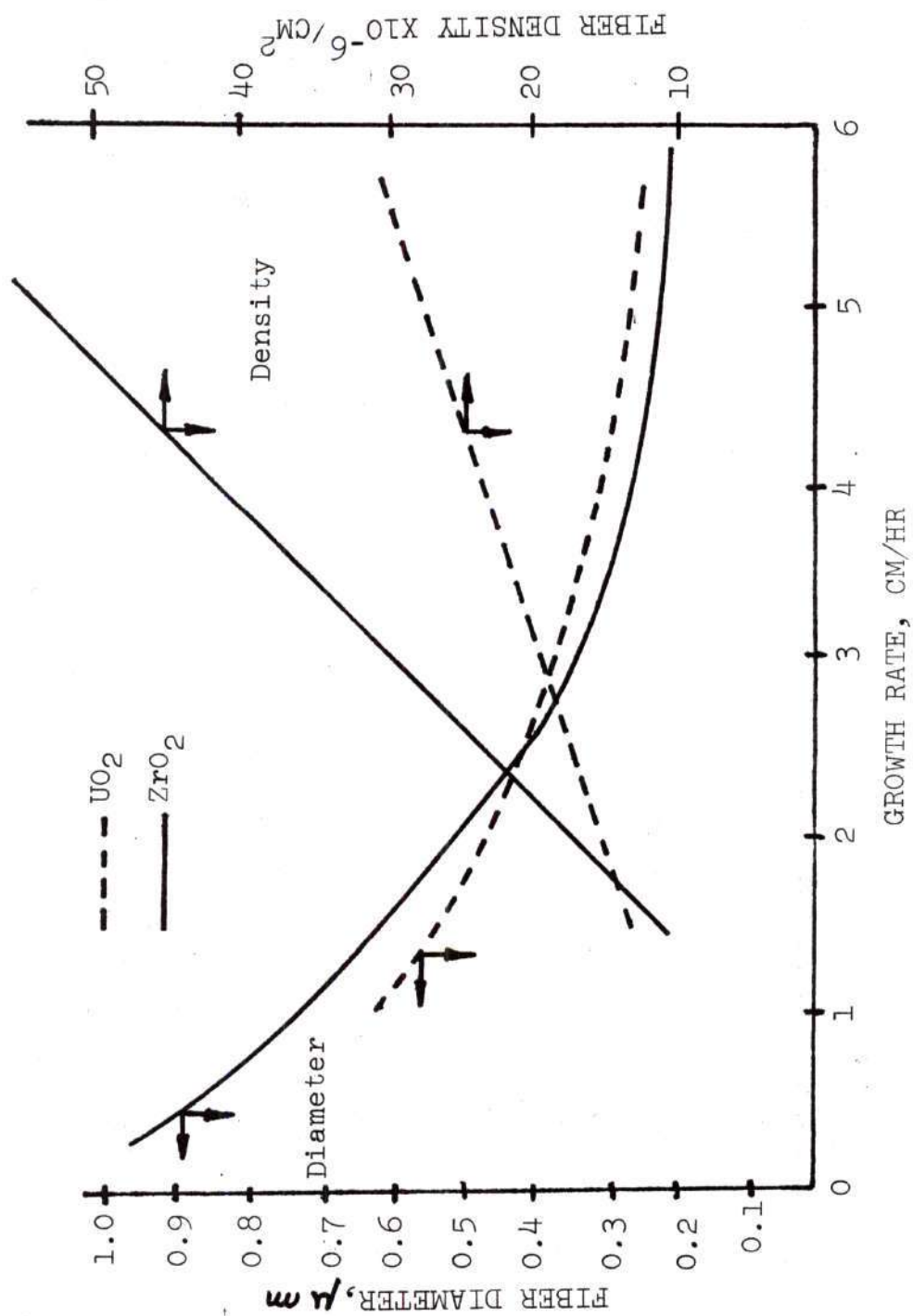


Figure 3. Effect of Growth Rate on the Fiber Diameter and Density in the Systems UO_2 -W, and ZrO_2 -W.

growth.

ZrO₂ Stabilized with CaO or Y₂O₃

Watson et al.¹³ successfully produced an ordered microstructure of W metal fibers in a CaO stabilized ZrO₂ matrix using the internal floating zone technique developed by Chapman. Reaction of the CaO with the W, however, made growth of large areas of composite impossible.

Later work by Watson^{14,15} proved that large areas of composite could be grown if Y₂O₃ was used as the stabilizer. A frequency of about 3.6 Mhz was found to give the best control over the growth operation. The amount of H₂ in the growth atmosphere was found to control the starting metal content that gave the best composite growth, but the effect was attributed to lower W vaporization at high H₂ contents rather than a change in oxide stoichiometry. Figure 3 shows that increasing solidification rate decreased fiber diameter and increased fiber density in the Y₂O₃ stabilized ZrO₂-W system.

HfO₂ Stabilized with Y₂O₃

Using techniques similar to Watson, Johnson^{14,16} successfully unidirectionally solidified Y₂O₃ stabilized HfO₂-W, producing an ordered oxide-metal composite. Fiber densities of up to 72×10^6 fibers/cm² were observed, but samples cracked badly during growth due to the high thermal gradient and low thermal shock resistance.

MgO and Cr₂O₃

Nelson and Rasmussen¹⁷ melted MgO and Cr₂O₃ in W, Re, and Mo crucibles and observed dissolution of the crucibles in the molten oxide and a tendency to form ordered metal fiber microstructures.

They speculated that the composite structures were apparently formed by the coupled solidification of the refractory metal fibers and the oxide from a binary oxide melt. Hart¹⁸ used the Bridgeman technique to grow composites in these systems, and tested them for mechanical strength.

Summary

At the present time the most uniform and largest oxide-metal composites have been grown using the direct rf coupling internal floating molten zone technique. The main advantage to that technique is that it eliminates containment and contamination problems inherent to other methods, however only a few refractory oxides possess sufficient stability and electrical conductivity to be used. Even with an oxide which has the needed characteristics, many factors must be controlled in order to produce a good sample. Chapman and his coworkers⁹ compiled the following list of parameters which influenced growth in refractory oxide-metal systems using the direct rf coupling technique:

1. Oxide-metal ratio
2. Growth rate
3. Metal powder characteristics
4. High-temperature electrical conductivity
5. Rf frequency
6. Mixing of the liquid (sample rotation)
7. Melting (eutectic) temperature
8. Preheat temperature
9. Sample density

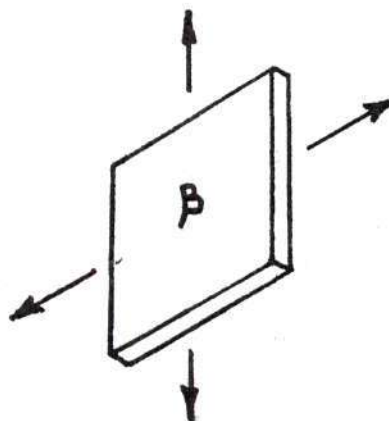
10. Sample rf-coil geometry
11. Quantity of liquid and void size
12. Oxygen partial pressure
13. Pre- and post-heater separation
14. Vapor pressure of the components
15. Variable oxide stoichiometry

Metal-Metal Solidification

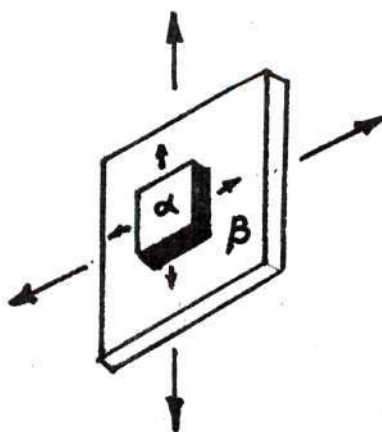
Due to the lack of theoretical work concerning the unidirectional solidification of oxide-metal mixtures, the literature analyzing metal-metal mixtures must be cited. Conclusions must be drawn carefully, however, because the two systems are more dissimilar than similar. Whereas only a condensed two phase system ideally needs to be considered in metal-metal solidification three phases must be considered in oxide-metal solidification, two condensed and one gaseous i.e. oxygen. Also, during solidification metal-metal systems undergo no bonding or other major changes. This is not true of oxide-metal solidification; the great effect of oxygen on metal solubility in the liquid oxide seen during solidification studies and shown in the system $\text{UO}_2\text{-W}$ by Latta and Frexel¹⁹, would indicate a loose ionic bonding of the metal with oxygen in the liquid, thus the metal must change to a metallic bond on solidification. In this section the nucleation and growth of eutectic structures is discussed along with the factors that control whether a rod or lamellar morphology is favored. An explanation of cellular growth, banding, and the coupled growth theory is also presented.

Any study of solidification processes should start with nucleation. Sundquist and Mondolfo²⁰ did a study of nucleation of eutectic alloys, and found that metals that had a complex structure were difficult to nucleate, and required large undercooling, but were good nucleation agents while metals with simple structures were easy to nucleate but were poor nucleating agents. In practice this means that the simple structured component would nucleate first, but the complex phase will not nucleate until growth of the simple phase has depleted the surrounding liquid of the simple phase causing a great enough undercooling to nucleate the complex phase. Once the growth of the complex phase has brought the liquid composition back to the eutectic, a halo of the complex phase is formed around the primary dendrite of the simple phase, and the simple phase is then renucleated by the complex phase. Once the simple phase is nucleated on the surface of the complex phase, a stable base is formed from which the eutectic will grow outward. Sundquist and Mondolfo²¹, in their paper concerning the nucleation of Pb found that no specific orientation relationship existed when one phase nucleated the other. This means that eutectic nucleation schemes like that proposed by Wiengard²² could not be possible since they require repeated nucleation events which would not give the specific orientation relationships observed between phases.

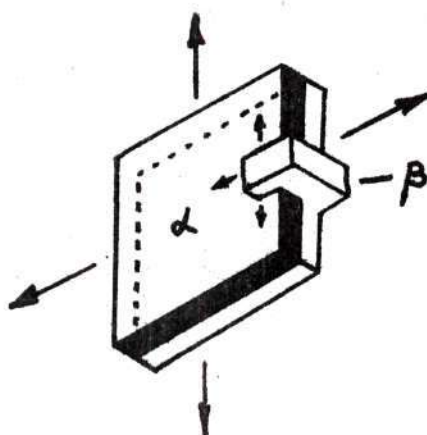
A bridging mechanism first proposed by Tiller²³ seems to be more likely. The first nucleus (simple phase), see Figure 4, which nucleates on the β phase halo will grow along the surface and normal to it. The width of the α phase is limited because of the enrichment



(a) Surface of the "halo" of Complex Phase



(b) First Simple Phase to Nucleate on the Halo.



(c) Bridging of the Simple Phase.

Figure 4. Nucleation of a Eutectic Grain By Bridging.

of the liquid adjacent to it with atoms of the β component thus enhancing the growth of the β phase. As the β lamella grows out it overlaps the α lamella that borders it giving rise to another β lamella of the same crystallographic orientation as the first. This process is repeated until alternate α and β lamella totally surround the β nucleus creating a growing nodule of eutectic alloy.

Subsequently, growth of the eutectic is governed by the need to minimize interphase spacing in order to reduce the diffusion distance at the solid-liquid interface, and the need to maximize interphase spacing so that the solid-solid interfacial area and therefore energy per unit volume is minimized. Several theories of lamellar growth have been proposed.²⁴⁻²⁶ The basis of these as shown in Figure 5 is that as the α lamella grows, the rejected B atoms build up ahead of the α phase (similarly the A atoms ahead of the β phase) until there is just sufficient lateral concentration gradient to transfer the rejected material across the interface. To do this a lateral concentration gradient similar to that shown in Figure 5 is needed. The different liquid compositions, C, at the liquid-solid interface gives rise to a variation in the undercooling, T_D , due to composition (T_D is defined as $m(C_E - C)$, where m is the liquidus slope and C_E the eutectic composition). The curvature of the lamellar tips will also effect the freezing temperature and is given by the Gibbs-Thomson relation in Equation 3.

$$\Delta T_C = \frac{\sigma}{\Delta S} \left(\frac{1}{r_1} + \frac{1}{r_2} \right) \quad (3)$$

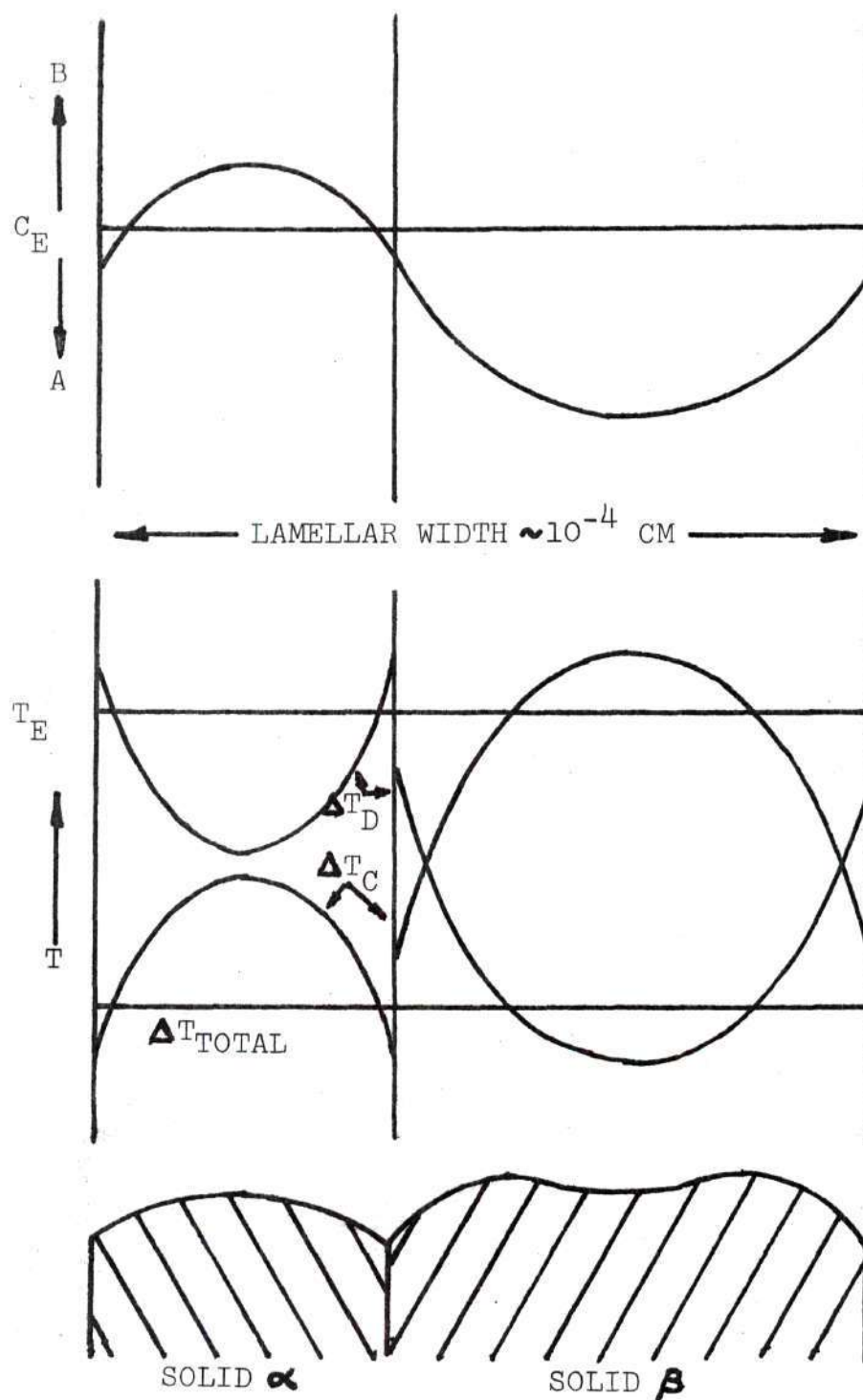


Figure 5. (a) A Schematic Concentration Profile of B over a Solid-Liquid Interface. (b) Contribution to the Total Undercooling Due to Composition and Curvature. (c) The Predicted Shape of a Lamellar Solid-Liquid Interface.

where ΔT_C = the undercooling due to curvature

ΔS = entropy of melting

σ = the isotropic solid-liquid interface energy

r_1 & r_2 = the principal radii of curvature

If we assume the total interface undercooling is constant across the interface and variation in ΔT_D must be balanced by a variation in ΔT_C as shown by Equation 4.

$$\Delta T \approx \Delta T_D + \Delta T_C = \text{constant} \quad (4)$$

Since ΔT_D has a minimum value near the liquid groove, the radius of curvature should be smallest in these regions, leading to a solid-liquid interface similar to that shown in Figure 5. Jackson and Hunt²⁷ extended the theory and obtained Equations 5 and 6 which interrelate the growth variables for lamellar and rod growth.

$$\Delta T/m = v \lambda Q^L + a^L/\lambda \quad (5)$$

$$\Delta T/n = v R Q^R + a^R/R \quad (6)$$

where v = the growth velocity

λ = the inter lamellar spacing

R = the inter rod spacing

and Q^L , Q^R , a^L , a^R and m are constants for a given alloy.

Rod-Lamellar Transition

Both rod and lamellar morphologies are favored by the short diffusion distance constraint on eutectic growth, but which morphology will be stable is the result of many interrelating factors, the most

important of which are volume ratio, growth rate, interphase boundary energy, and impurities. Tiller²⁴ hypothesized that the rod morphology would be favored by a high volume ratio between the two phases.

Chadwich²⁸, however, pointed out that even though a change from a lamellar to a rod structure can reduce the interphase boundary area if the volume ratio between the two phases is greater than 2 to 1 there will not be a corresponding decrease in interphase boundary energy since interphase boundary energy can vary with orientation. It would be possible for lamella in certain orientations with respect to each other to have a lower boundary energy than the average boundary energy of the rod morphology, which would tend to stabilize the lamella.

Lemkey et al.²⁹ found that a rod-plate transition could be induced in Al-Al₃Ni by varying the growth rate with rods being favored at the higher growth rates. Cooksey et al.³⁰ working in the same system tried to relate the transition to the lead distance of one phase over the other. He said that an increase in growth rate or a decrease in temperature gradient would increase the lead distance thus promoting bridging of the leading phase over the lagging one, producing a rod structure.

Hunt and Chilton³¹ showed that if the lamella were forced to bend out of their own plane, the low energy interface that stabilizes the lamellar structure would be lost. In the six eutectics tested they found that if the volume fractions were less than $1/\sqrt{2}$, then the lamellar structure is deprived of its energy advantage and a fiber structure would be favored. In practice the solid-liquid interface

can become curved for a variety of reasons, the most important of which is at colony boundaries. Hunt explained that at the center of the colony the lamellae can lie paralleled to each other and to the growth direction, while growing normal to the liquid-solid interface. However, toward the sides they must curve outward to accommodate the increasing interface curvature so that the departure from the preferred lamellar plane becomes energetically favorable. Chadwich²⁸ pointed out, however, that Hunt and Clintons criteria did not explain why lamella growing normal to the cell boundaries can be made to transform to the rod-type structure if enough impurity is present, and lamella are not always modified at colony boundaries. Chadwich states that the rod-lamella transition occurs when the eutectic alloy contains an impurity element which has different partition coefficients in the two eutectic phases. He showed that if one phase α has a lower partition coefficient for a given impurity than the other phase β that during solidification there will be a buildup of impurity ahead of the α phase since the α phase will reject more impurity element than the β phase. As a consequence of this impurity buildup the equilibrium freezing point of the liquid in contact with the α phase is lower than the liquid in contact with the β phase. Therefore the β phase will grow a finite distance ahead of the α phase. Since the liquid ahead of the α lamella is supercooled with respect to the α phase any portion of the α phase which happens to grow ahead will become stabilized. The impurity rejection from this protrusion will then be radial and bridging

across the α lamella by the β lamella is then possible causing a break-down to a rod structure. In impure eutectics where there is a colony structure, and the rod morphology occurs only at colony boundaries, the partition coefficients change with changing impurity levels.

Cellular Growth

Ideally the grown eutectic structure should be uniform across the liquid-solid interface. However, in practice the structure is broken up by a cellular structure which is generally 2-3 orders of magnitude larger than the eutectic structure. When a eutectic grows with a cellular structure, the microstructure does not grow parallel, but diverges toward the cell walls. Chalmers³² has shown that a cellular structure is due to impurities, and can be explained in terms of constitutional undercooling. In the case of a planar interface the undercooling would occur as a gradient of supercooling from the interface into the liquid. In such a gradient the planar interface would be unstable, because if any localized area advances ahead of the general interface it becomes stabilized. Such a region would grow as a protuberance until as a result of the gradient of supercooling combined with its evolution of latent heat it encounters a region where the supercooling is only sufficient to provide the necessary driving force for growth. The rejection of impurities causes a buildup at the base of the protuberance which retards solidification in this region so the protuberance cannot expand laterally. The convexity caused at the base by the impurity buildup triggers similar protuberances around the original one, and the result

is an array of cells having an approximately close packed structure.

Chalmers made three qualitative predictions about cell behavior:

1. The cell surface is convex toward the liquid.
2. The concentration of impurities is higher at the cell walls than in the cell centers, and is at a maximum where cell boundaries meet.
3. Cell formation can be suppressed by reducing the impurity content, reducing the speed of growth, or increasing the temperature gradient to eliminate the region of supercooling.

Hunt and Jackson³³ have observed these predictions to be true during growth of low temperature organic eutectics.

Banding

Transverse banding has been often observed in unidirectionally solidified eutectics. A transverse band consists of a narrow disruption by an area of non-coupled growth of the coupled eutectic growth, perpendicular to the growth direction. Usually this area consists of disordered eutectic or dendritic growth which requires renucleation of ordered eutectic growth. However, narrow bands have been observed in oxide-metal eutectics which are composed of one phase, and do not require renucleation.

Chadwich³⁴ stated that banding could be produced by any deviation from steady state growth conditions. He said that although an off eutectic alloy would grow under steady state conditions without the formation of the primary phase, this was not true when the growth rate changed suddenly. At that point the primary phase

precipitated on the growth front causing a band. In practice many things can cause non-steady state growth. Kaneko and Flemings³⁵ listed the ones they considered most important as follows:

1. The mechanical device which drives the furnace or specimen container is not operating smoothly. This becomes important at slower growth rates.
2. Fluctuations in power supplied to the furnace.
- 3) Mechanical shock or vibration of the sample.
- 4) Fluctuations in flow rate or temperature of cooling media.
- 5) Temperature fluctuations due to turbulent convection in the melt.

Coupled Zone

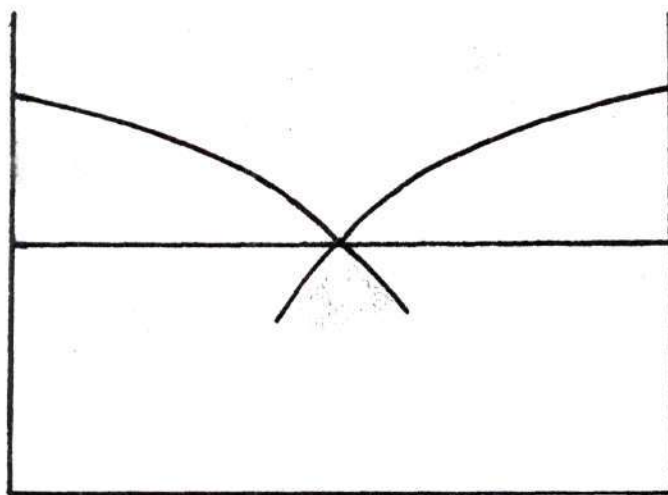
The theory of cooperative or coupled growth was first presented by Scheil²⁶ and later expanded by Hogan³⁶ and Tiller²³. Only a qualitative explanation of the theory will be presented here. At zero growth rate (equilibrium) only the eutectic mixture can produce the eutectic structure without primary phase dendrites. At finite growth rates equilibrium conditions do not exist and a range of compositions can solidify with the eutectic structure. This range can be thought of as a metastable zone below the solidus line of a conventional phase diagram as seen in Figure 5. The width and shape of the coupled zone can be explained in terms of growth velocity of the two phase region being faster than any of the component phases independently. Thus, when the primary phases are nucleated their growth is stifled because the eutectic growth quickly engulfs them. Outside of the coupled region one primary phase grows first until

the liquid is sufficiently enriched in the other to bring it into the coupled region. If the two pure phases have identical melting points, the coupled region will expand below the eutectic point and have a symmetrical shape as seen in Figure 6a. If the component phases have widely different melting points the zone will no longer be symmetrical, but will be skewed toward the higher melting phase as shown in Figure 6b. This effect is due to the greater supercooling of the high temperature phase versus the low temperature phase, thus the temperature dependence of growth velocity is greater for the high temperature phase.

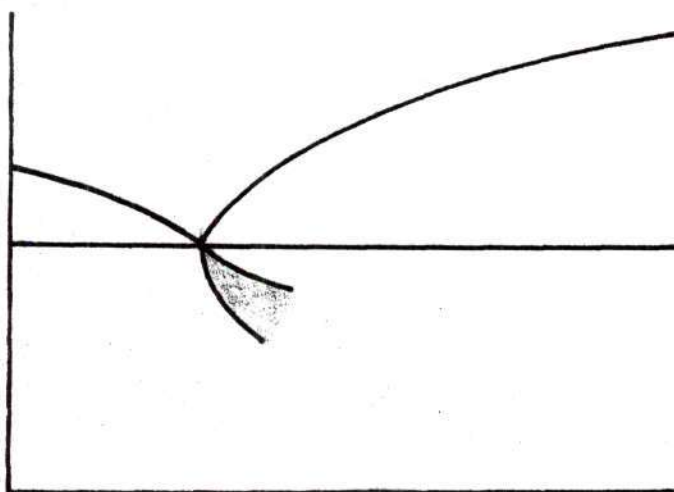
The practical significance of the coupled zone theory has not been fully explored, but two obvious points are worth mentioning. First the solidifying mixture does not have to be exactly at the eutectic composition to produce a structure free of primary dendrites, and second at increasing growth rates the quantity of the higher melting phase needed for coupled growth will tend to increase.

Rare Earth Oxides

The rare earth elements are generally referred to as those elements between atomic numbers 57 and 71 on the periodic chart. Very little was known about the rare earths until recently because it wasn't until the late forties³⁷ that methods were devised to separate the various elements in quantities greater than a few grams. Since that time many uses for the rare earths have been discovered and the cost has steadily declined even with increasing demand due to improved separation methods.



(a) The Coupled Zone in a System that has Components of Similar Melting Points.



(b) The Coupled Zone in a System that has Components of Different Melting Points.

Figure 6. Conventional Phase Diagrams Showing the Sub-Solidus Coupled Zone.

Most of the rare earth oxides are promising ceramic materials. The most stable form for most of the rare earth oxides is the R_2O_3 or sesquioxide. Ceria is stable as the dioxide, and the accepted formulas for terbium and praseodymium oxides are Tb_4O_7 and Pr_6O_{11} respectively. Europium, although stable as the sesquioxide, is easily reduced to EuO . The sesquioxides are very stable, and will only go slightly substoichiometric³⁸ at high temperatures in reducing atmospheres. They are very refractory with melting temperatures in all cases above $2000^{\circ}C$. Upon exposure to the atmosphere they absorb CO_2 and H_2O , this behavior is more pronounced with the lighter rare earth oxides; and becoming negligible with the heavier ones. They are insoluble in water, but are easily dissolved by mineral acids. Thermoanalysis³⁹ of cooling curves shows (see Figure 7) that the sesquioxides undergo several phase changes with an accompanying volume change on cooling. Ceramic studies^{40,41} of the rare earth oxides show that they sinter easily to high density, and react with many of the common ceramic oxides when heated with them to $1500^{\circ}C$.

Ceria although stable in the dioxide at ambient conditions goes substoichiometric in reducing atmospheres at high temperatures. Bevin and Kordius⁴² studied the stoichiometry of CeO_2 at various O_2 pressures up to $1160^{\circ}C$ and proposed the composition versus temperature diagram in Figure 8. X-ray work⁴³ in the system Nd_2O_3 - CeO_2 indicates that Nd_2O_3 goes into a substitutional solid solution with CeO_2 up to 75 percent sesquioxide. Above this percentage there is a two phase region of sesquioxide and solid solution.

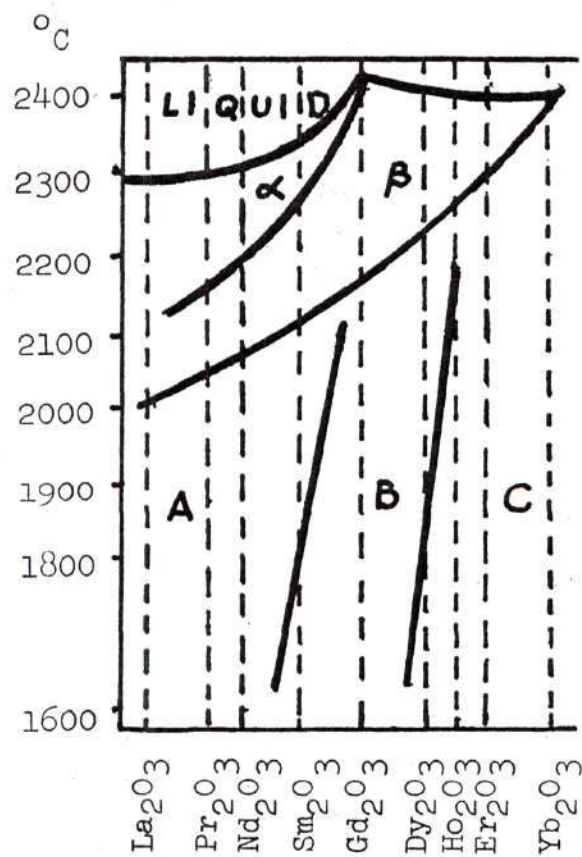


Figure 7. Phase Transformations of Rare Earth Sesquioxides, Detected by Thermoanalysis of Cooling Curves. α β are Stability Regions of High Temperature Phases, A, B, C are Regions of the Known A-, B-, C-type Polymorphs.

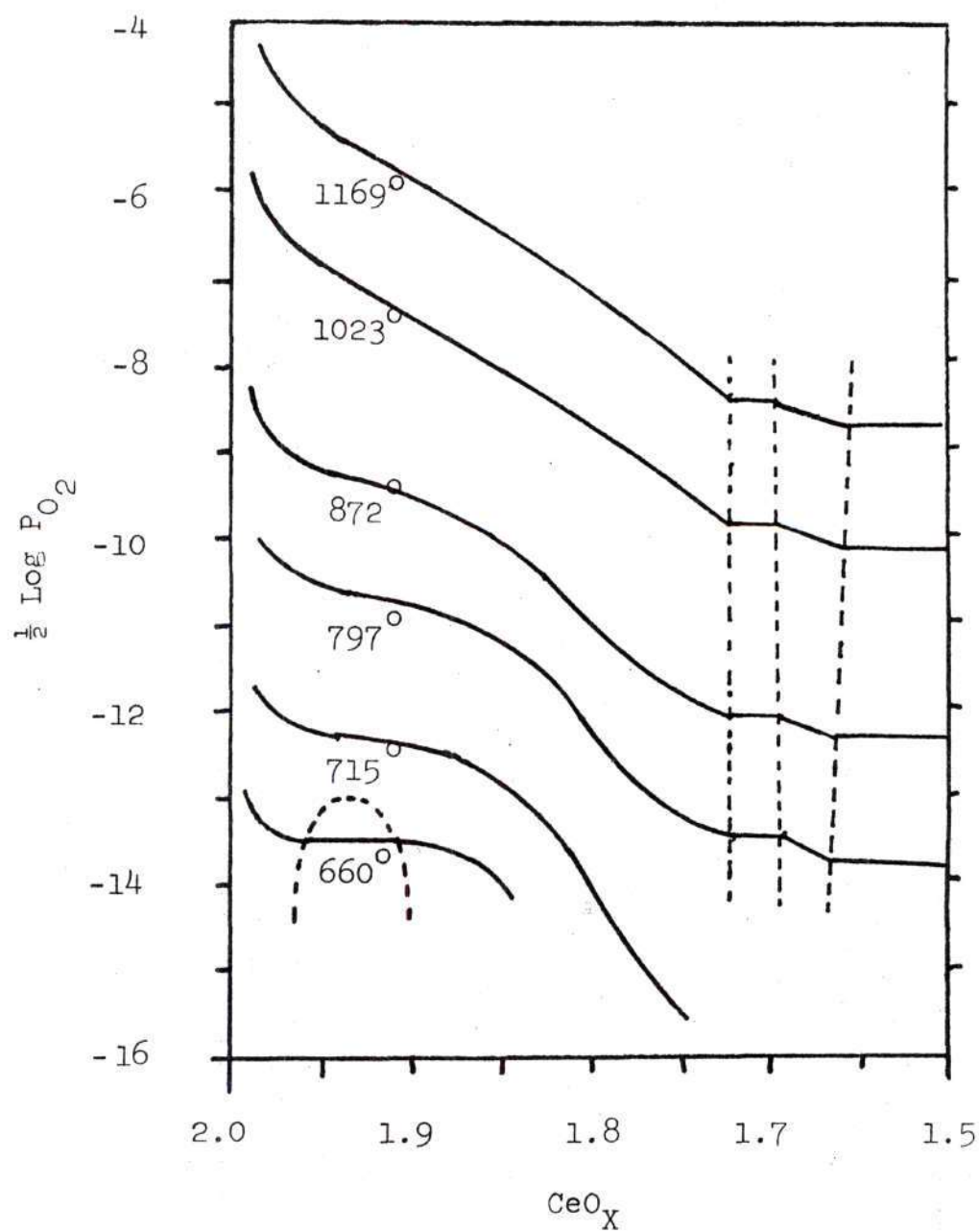


Figure 8. Equilibrium Oxygen Partial Pressure as a Function Ceria Composition for Temperatures of 660 to 1169°C, (After Bevin and Kordis⁴²).

CHAPTER III

EQUIPMENT

This section describes the equipment used in the production of rare earth oxide-metal composites. The Lepel induction heating unit, and the growth lowering apparatus is the most important part of this equipment, and will be described in detail. Other apparatus used for pellet fabrication and sample examination was less important and will not be described.

Induction Heating Unit

The induction heating unit used in this investigation was a Lepel high frequency generator, Model number T-10-3-DF1-E-HW, type T-1003-58, serial number 7023. The generator was the vacuum tube oscillator type rated at a 10 kilowatt output, and capable of operating over a wide frequency range. During this investigation frequencies between 3.5 and 4.0 were used, because this was found to be the best frequency range for growth. Tuning of the unit to match the work load was accomplished with a variable grid coil which could be adjusted during operation. Plate current and voltage readings were used as guidelines to control the power settings used, and determine the status of the pellet. The work coil was fabricated from rectangular copper tubing 1/8 by 1/4 inch. The coil itself was 1-3/4 inches inside diameter, and was 2-1/2 inches long, with 6-1/2 turns of tubing.

Growth Apparatus

The growth apparatus served the dual purpose of controlling the atmosphere and the position of the Mo heaters and sample in relation to the coil. The heart of the apparatus is shown during growth of a sample in Figure 9, and drawn in cross section in Figure 10. The brass base supported the silica tube which was used for atmosphere containment. A high alumina refractory support held the bottom Mo heater, and a hollow stainless steel rod through which the exhaust gas flowed held the top Mo heater. The sample was supported by the Nd_2O_3 spacer pellet which in turn was supported by an alumina tube which fit over a steel shaft that was connected to a hydraulic cylinder. A series of valves controlled the hydraulic cylinder so that it and in turn the sample could be raised and lowered at rates of from near zero to about 100 cm/hr. The silica tube and bottom Mo heater could be moved independently of the sample by lowering the table they were mounted on. The top Mo heater could be moved independently by sliding the steel support tube through the rubber stopper. Atmosphere gases were controlled with flow meters, were mixed, and passed through the brass base into the silica tube. The gases exited through the top Mo support rod and passed through a bubble bottle to prevent back diffusion before being exhausted into the air.

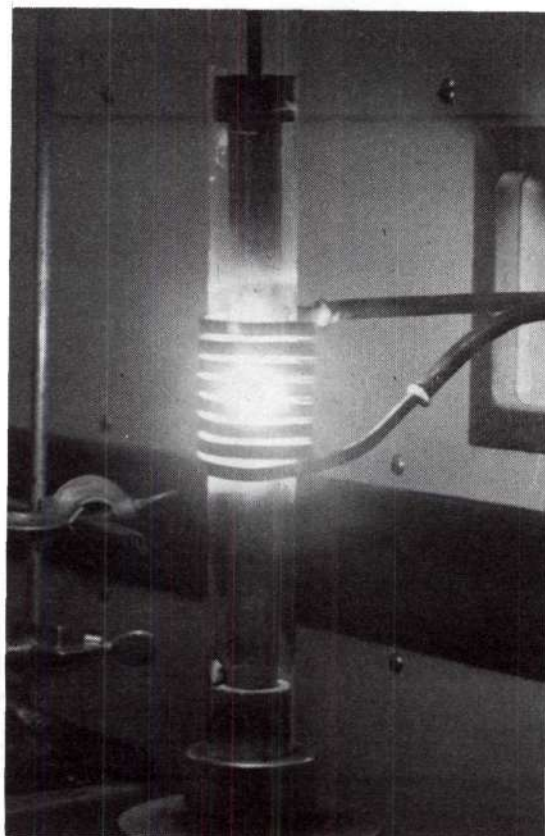


Figure 9. Induction Heating Facilities Used for Growth of Rare Earth Oxide-Metal Composites.

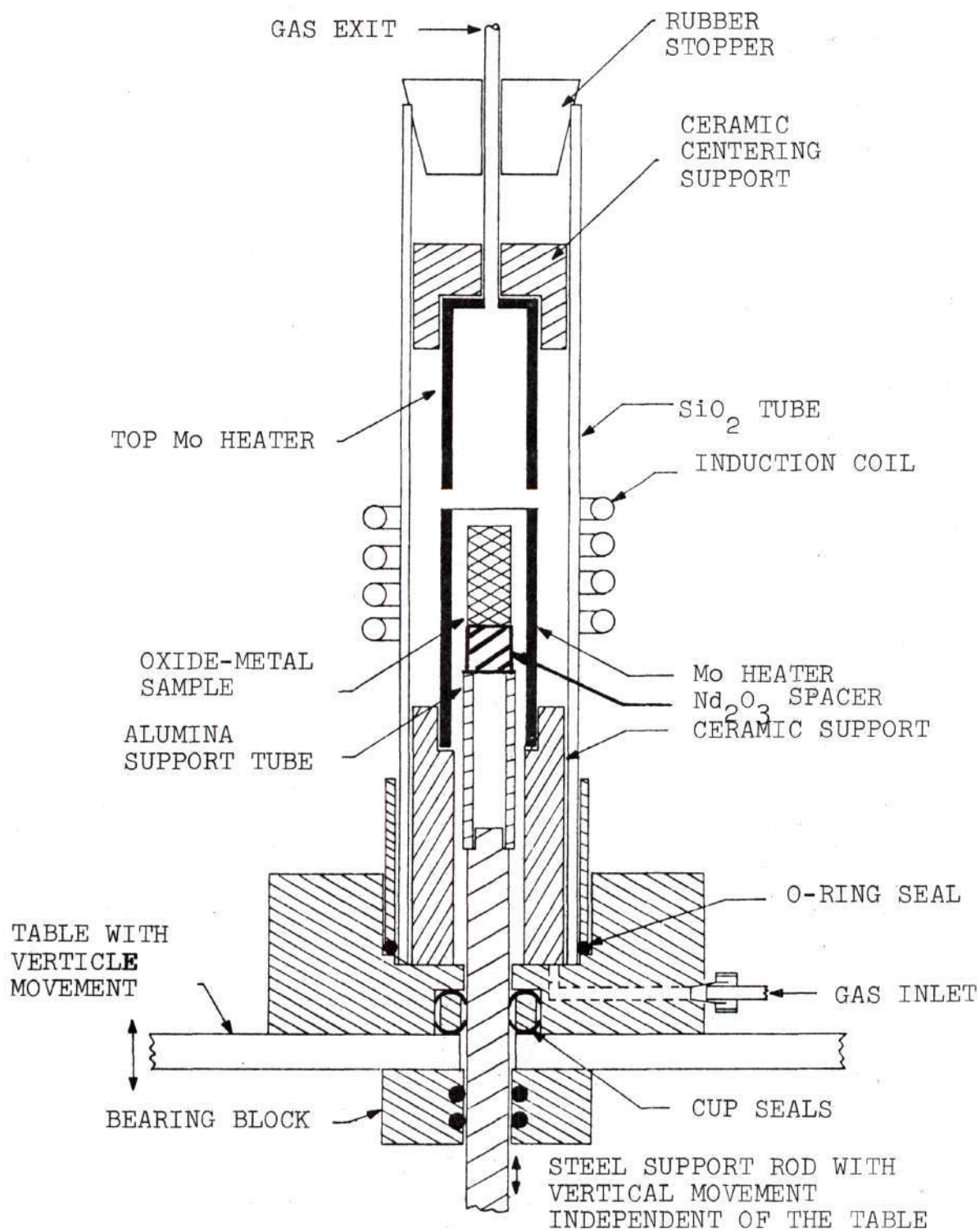


Figure 10. Schematic Diagram of the Facility for the Growth of Oxide-Metal Composites.

CHAPTER IV

GROWTH PROCEDURE

This section discusses the procedure used for growing rare earth oxide-metal composites. The procedure occasionally deviated from what will be discussed here when it was necessitated by the study of a growth variable. However, most of the best composite structures were grown using this general procedure. Each individual pellet constituted an experiment, and usually passed through three distinct phases; preparation, growth and examination. The growth procedure was by far the most critical part of the procedure, and will be discussed in the greatest detail.

Pellet Preparation

The first step in the fabrication of the green pellets used in this investigation was to calcine the as received oxide powders, except for CeO_2 , to about 800°C to drive off water of hydration. This was accomplished by heating the powder in a small fireclay crucible with an electric furnace. As soon as the powder reached 800°C it was removed from the furnace and allowed to cool. Storage of the calcined powders and grown samples to prevent rehydration was effected by keeping them in a small vacuum chamber which was kept continuously evacuated with a mechanical pump.

The second step in pellet fabrication consisted of mixing and pressing the specific composition to be melted. The oxide and metal

powders needed for each pellet were weighed to the nearest 0.1 g and thoroughly mixed in a porcelain mortar. The mixed powder was then pressed into pellets using one of two methods, uniaxial, or isostatic pressing. Most of the early experiments with pure oxides, pure oxides plus metal, and nearly all of the samples with Nd_2O_3 as the major constituent were uniaxially pressed in a steel die to approximately 560 Kg/cm^2 to produce a 1.87 cm diameter by 3.81 cm long pellet. The majority of the samples run with Gd_2O_3 as the major constituent were fabricated by placing the mixed powder into a thick walled rubber die and isostatically pressing to 4000 Kg/cm^2 . Isopressing in contrast to uniaxial pressing produced pellets slightly larger in diameter, about twice as long, and of uniform density. Isopressing was used when samples over 4 cm long were to be grown. If long rods were uniaxially pressed the middle sections were compacted less than the ends so that when it was sintered prior to melting the pellet had an hourglass shape. Since rf coupling efficiency decreased with decreasing diameter the power requirements to keep a stable molten zone in such an hourglass pellet changed as the pellet was lowered, making it impossible to solidify the entire length of the pellet without power setting changes which would disrupt the fiber growth. Isostatically pressed pellets, on the other hand sintered into uniform cylinders making power changes during growth unnecessary.

The materials used in this investigation came from three main sources. The Mo powder came from Wah Chang, lot number Mo-1008, and except for about 0.05 percent oxygen all impurities tested for were well below 0.01%. The rare earth sesquioxides were obtained from Kerr

McGee Chemical Company and were their 99 percent pure grade. Cerium powder was purchased from Fisher Chemical Supply Company and was their reagent grade.

Growth Procedure

Growth of the composite was divided into five main steps; set-up, preheat, coupling, lowering, and slow cooling. Set-up consisted of placing the prepared pellet in the growth-lowering apparatus shown in Figure 9. The Nd_2O_3 spacer pellet was used to keep the rare earth alumina interface, which reacts at a low temperature, below the hot zone, while raising the sample pellet high enough to melt at the bottom and obtain maximum solidification length. Care had to be taken during the set-up to insure proper centering of the sample, Mo heaters, and quartz tube in the coil or arcing would result once high power was applied. After the sample was loaded into the apparatus, a dynamic atmosphere of about 10 vol% H_2 and 90 vol% N_2 flowing at about 500 cc/min was introduced. At that point rf power was applied and slowly increased, with an automatic controller, over a period of an hour, which heated the bottom Mo tube gradually to approximately 1750°C . It should be noted that temperatures cited are only approximate due to the fact that no correction was attempted for emissivity, and radiation losses through the SiO_2 tube wall and vapor deposits often seen on the tube wall.

After the sample was preheated it was ready to be directly coupled to the rf field and melted. The coupling operation was the most difficult part of the growth procedure since to be successful it

had to be executed with a minimum of error in less than a minute. The reason for this difficulty was that the conductivity of the sample was very low even at the preheat temperature, and nearly full power had to be applied to establish a molten zone; thus neither Mo susceptor could be in the coil when the sample was initially melted. Also once the molten zone was established both Mo tubes had to be placed back into the coil trapping the zone between them so the movement of the molten zone could be precisely controlled. The coupling procedure itself consisted of three main phases; lowering the bottom Mo heater from the coil, melting the pellet and repositioning both Mo heaters. From the preheat position the bottom Mo was quickly lowered from the coil as the rf power was slowly reduced so that a low value was reached as the top of the tube cleared the coil. The tube was lowered farther to a position about 3 cm below the coil as the power was raised back to near the maximum available. Once direct rf heating occurred and a molten zone was established the power was reduced to a low value, and the two Mo heaters positioned so as to trap the hot zone in a 26 mm gap between them. This was the most difficult part of the operation, and a neck had to be developed to know when the molten zone was initially established so the power could be reduced in time to prevent excessive melting and siphilage. During the coupling procedure it was often useful to use the plate voltage and current meters as aids. Plate current was directly responsive to the power control knob, and was the truest indicator of power input. Plate voltage, although responsive to the control knob also responded to the conductivity of the pellet. If the pellet was molten the plate voltage was low for

the current setting, and conversely if the pellet was solid the voltage was high for the current setting. During coupling the voltage drop concurrent with the first melting could be used to tell when the power should be cut back to avoid spilling. The final step in the coupling procedure was to raise the rf power settings to a value, which had been previously determined by trial and error, to keep a specific composition melted without spilling. In most cases this meant keeping the skin temperature of the pellet around 1800°C because it was found that at temperatures above 1900°C spilling occurred and at temperatures below 1700°C the molten zone solidified. Temperature control was affected by minor adjustments in the rf power.

The actual growth of the sample was accomplished by slowly lowering the pellet from the coil. The molten zone could not move in relation to the coil because it was pinned between the Mo tubes which were stationary during growth. Once the pellet had been lowered until the top was entirely inside the bottom Mo tube the rf generator was again placed on automatic control and the power slowly lowered over a period of an hour, so as to slow-cool the sample and prevent thermal shock.

Examination

After growth most samples were sectioned longitudinally and transversely with a diamond saw. The sections were then ground with silicon carbide paper, and polished with $1\mu\text{m}$ diamond paste on a nylon cloth. The polished sections were then microscopically examined at 30 and 600X. It was found that 30X was best for determination of cell

structure, amount of banding, and over-all pellet appearance, and that 600X was best for examination of the fiber morphology, and the details of the fiber array.

CHAPTER V

DISCUSSION AND RESULTS

The initial objective of this investigation was to find new systems in which ordered oxide-metal structures could be grown using the direct rf coupling floating internal molten zone technique. This goal was quickly reached with the successful unidirectional solidification of a Nd_2O_3 -Mo composite sample. The emphasis of the investigation then shifted to improving the composite structure so that samples suitable for field effect electron emission testing could be produced. This goal was also reached and emission test data has been reported.⁹ The emission testing of rare earth oxide-metal composites was conducted by other investigators and this area will not be discussed. A large number of different rare earth oxide-metal combinations were tried to explore what systems could be successfully grown. This work is summarized in the first section along with a general description of the composite. The systems Gd_2O_3 - CeO_2 -Mo and Nd_2O_3 - CeO_2 -Mo were studied in more detail to characterize growth parameters. The more important findings of this investigation are presented in the second section. Etching techniques were developed in order to produce different fiber geometries for emission testing, and the results are illustrated in the last section.

Composite Growth in the Rare Earth Oxide Metal Systems

A brief summary of the different rare earth oxide-metal combinations which were tried and the results are given in Table 1. All of the sesquioxides which were successfully induction melted and unidirectionally solidified had essentially the same growth characteristics and composite geometry when the same metal was used. Therefore, results for one of these oxides can be broadly applied to the others. Burke⁴⁴ completed the investigation of the pure CeO_2 metal systems initiated during this work.

Two typical samples longitudinally sectioned after growth are seen in Figure 11. The longer sample was isostatically pressed, the other uniaxially pressed. The dark areas in the pellets are the solidified areas which are surrounded by the unmelted base and skin. The void at the top of the melted area is due to the difference in porosity between the sintered and melted material. At the bottom of the melted zone there is a disordered area containing large metal blobs, and non-uniform composite growth. Above this is the area of uniform fiber growth which extends to the void. Typical transverse and longitudinal microstructures of good fiber areas are shown in Figure 12. The uniform composite is interrupted by a grain or cellular substructure which divides the composite into irregular areas which are generally 0.1 to 1 mm in diameter. A typical boundary is shown in Figure 13. It is unknown if this boundary separates grains, where a crystallographic change occurs or cells, where no crystallographic change occurs. It is felt that it is a grain boundary since abrupt fiber morphology changes are occasionally seen across these boundaries

Table 1. Summary of Composite Growth in the
Rare Earth Oxide-Metal Systems.

| Oxide | Metal | Description of Composite Structures | |
|---------------------------------------|-------|-------------------------------------|--|
| Nd_2O_3 | Mo | Poor Fiber Continuity | Slowly Hydrated |
| | W | Poor Fiber Continuity | |
| | Nb | Unstable Zone | |
| | Ta | Unstable Zone | |
| $\text{Nd}_2\text{O}_3(\text{CeO}_2)$ | Mo | Good Fiber Structure | Matrix Slowly Hydrated |
| | W | Good Fiber Structure | |
| La_2O_3 | Mo | Poor Fiber Continuity | Matrix Rapidly Hydrated |
| | W | Poor Fiber Continuity | |
| $\text{La}_2\text{O}_3(\text{CeO}_2)$ | Mo | Good Fiber Structure | Matrix Rapidly Hydrated |
| | W | Good Fiber Structure | |
| $\text{Er}_2\text{O}_3(\text{CeO}_2)$ | Mo | Good Fiber Structure | |
| $\text{Ho}_2\text{O}_3(\text{CeO}_2)$ | Mo | Good Fiber Structure | |
| CeO_2 | Mo | Good Fiber Structure | Structure Depen- dent on Oxide Stoichiometry |
| | W | Good Fiber Structure | |
| Gd_2O_3 | Mo | Did Not Couple | |
| $\text{Gd}_2\text{O}_3(\text{CeO}_2)$ | Mo | Good Fiber Structure, No Hydration | |
| | W | Good Fiber Structure, Zone Unstable | |
| | Cu | No Fibers | |
| | Rh | No Fibers | |

Table 1. (Continued)

| Oxide | Metal | Description of Composite Structures |
|-------------------------|-------|---------------------------------------|
| Dy_2O_3 | Mo | Did Not Couple, Possible Phase Change |
| Sm_2O_3 | W | Did Not Couple, Slowly Hydrated |
| Y_2O_3 | Mo | Did Not Couple |

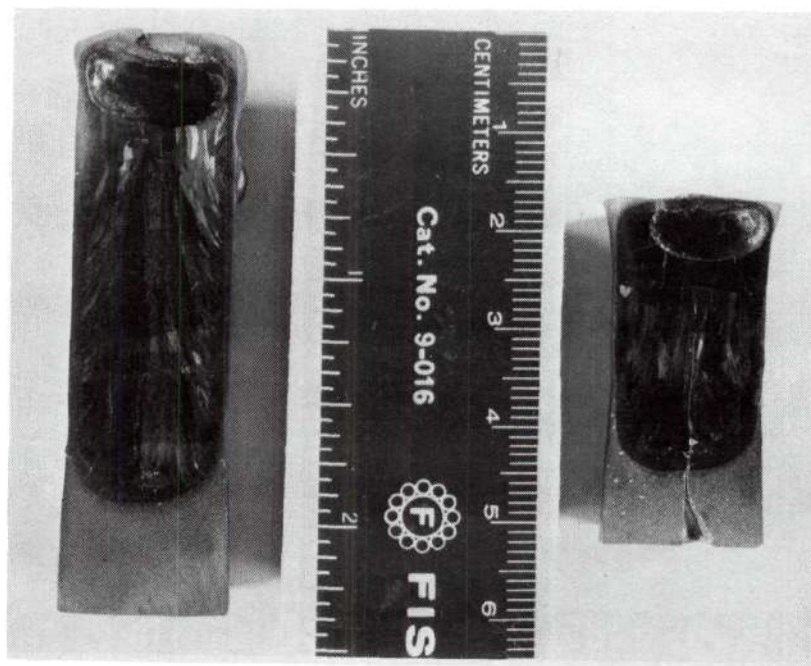
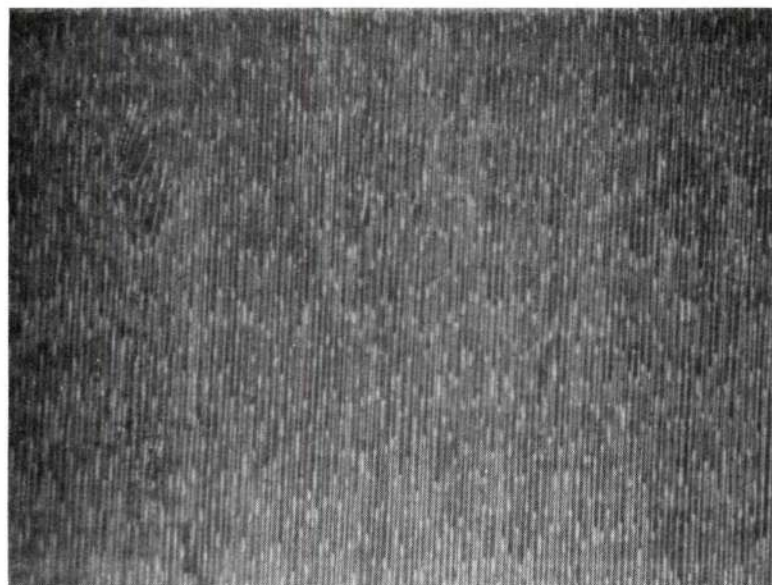
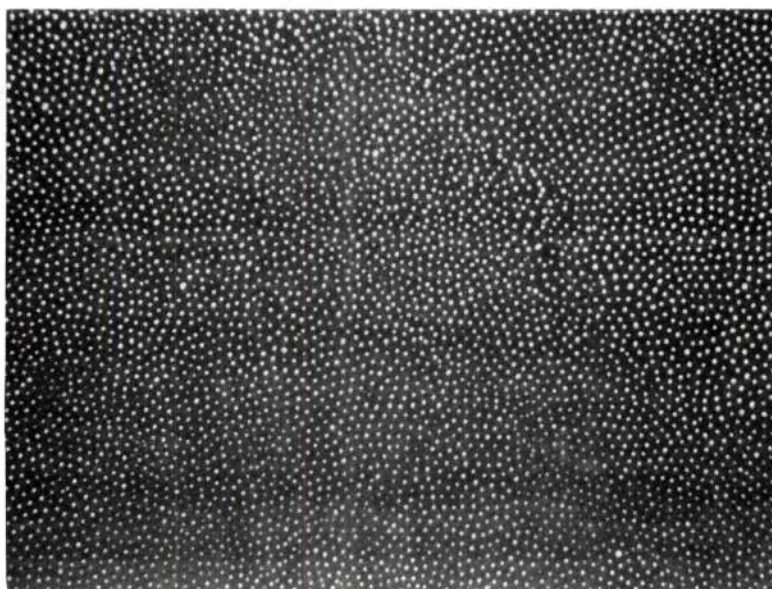


Figure 11. Macroscopic View of Two $\text{Gd}_2\text{O}_3\text{-CeO}_2\text{-Mo}$ Samples Which have been Longitudinally Sectioned After Growth. The Pellet on the Right was Uniaxially Pressed While the Left Hand Pellet was Isostatically Pressed.



(a) Longitudinal Section



(b) Transverse Section

Figure 12. Transverse and Longitudinal Sections of "Good" Fiber Growth in the System $\text{Gd}_2\text{O}_3\text{-CeO}_2\text{-Mo}$. This Type of Growth is Typical For All the CeO_2 Doped Rare Earth Oxide-Metal Systems. Dark Field, X600.

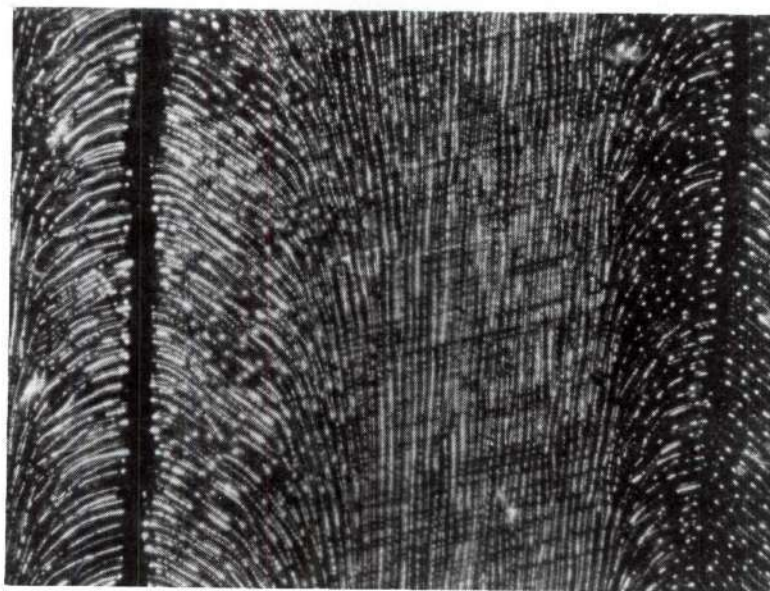


Figure 13. Transverse Section Showing a Distinct Boundary. Note How the Fibers Curve Out Toward the Boundary. Growth Direction is Toward the Top of the Paper. Dark Field, X600.

indicating a crystallographic change.

Molybdenum and tungsten gave very nearly the same composite geometry with W samples tending slightly more toward the short lamellar-fiber morphology. Tungsten samples, unlike Mo samples, were difficult to successfully unidirectionally solidify due to the narrow range of power settings available between maintaining a stable molten zone and melting through the skin. No other metal tested (see Table 1) gave any indication of coupled composite growth. Lack of metal solubility and reactions between the metal and oxide were the main difficulties.

Minor variation of the growth atmosphere made no noticeable change in the grown rare earth oxide-metal composite structures. Samples grown in pure N_2 exhibited good structures, but vapor deposits on the quartz tube were more pronounced which caused difficulties with coil to sample arcing. Samples solidified in N_2 - H_2 mixtures containing above 50% hydrogen generally exhibited poor structures. This is probably due to reduction of CeO_2 prior to melting causing low oxygen content and poor metal solubility.

Effect of CeO_2 Additions

Work in the system UO_2 -W^{9,19} showing the importance of hyperstoichiometry on tungsten solubility, suggested that the poor structures seen in the rare earth sesquioxide-metal systems (without CeO_2 additions) was caused by low metal solubility due to a low oxygen content of the molten oxide. Small additions of CeO_2 were made to the sesquioxides in the hope that the CeO_2 would go into solid solution with the sesquioxides during solidification, and provide extra loosely

bound oxygen to increase metal solubility in the molten oxides. Figure 14 shows the dramatic improvement in fiber structure with a twenty percent addition of CeO_2 to the Nd_2O_3 -Mo system. X-ray analysis of the composite areas in a series of Nd_2O_3 - CeO_2 -Mo samples grown with CeO_2 additions between 10 and 30 wt% indicate that ceria forms a substitutional solid solution with the hexagonal Nd_2O_3 structure. Figure 15 shows how well Vegard's⁸ law is followed. This behavior appears to differ from the results of Mozzi and Guentert⁴³, but the reduction of the ceria to the sesquioxide in the growth atmosphere most likely allowed it to fit in the Nd_2O_3 structure. Examination of these samples showed no difference in composite geometry, but differences in melting and solidification characteristics were noted. As the CeO_2 content was increased the following effects were noted:

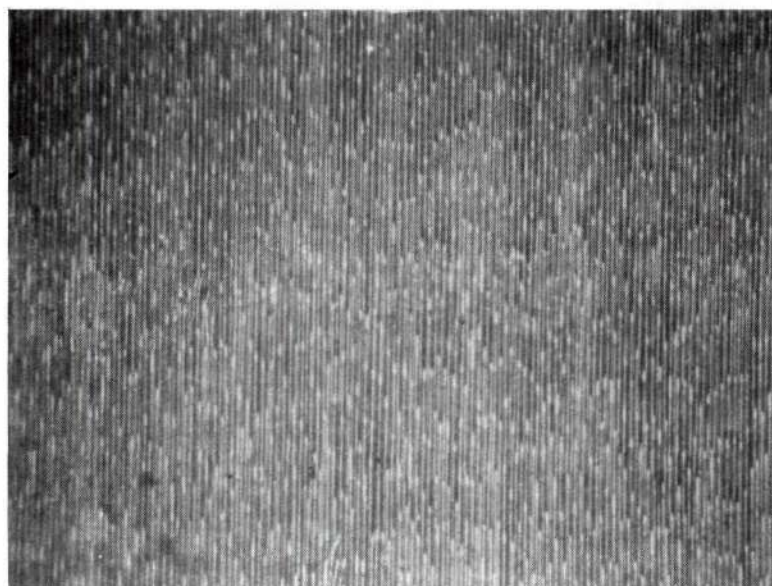
1. The stability of the molten zone was increased.
2. Susceptibility of samples to cracking due to thermal shock was increased.
3. Preheat temperature required to obtain direct rf coupling decreased (electrical conductivity of the unmelted pellet increased).
4. Power requirements to maintain a molten zone increased (electrical conductivity of the liquid decreased).

On the basis of these runs it was decided that compositions containing about 20 wt% CeO_2 were the easiest to control during growth, and gave the best composite structures.

The results of a sample in which the molten zone was passed through the pellet twice indicated that the role of cerium is to hold oxygen in the system until the oxide-metal feed mixture melts. The



(a) Sample Without CeO_2 Addition



(b) Sample with CeO_2 Addition

Figure 14. Longitudinal Sections Comparing the Fiber Growth in Nd_2O_3 -Mo Samples with and Without CeO_2 Additions, (Note the Dramatic Improvement in Fiber Structure). Dark Field, X600.

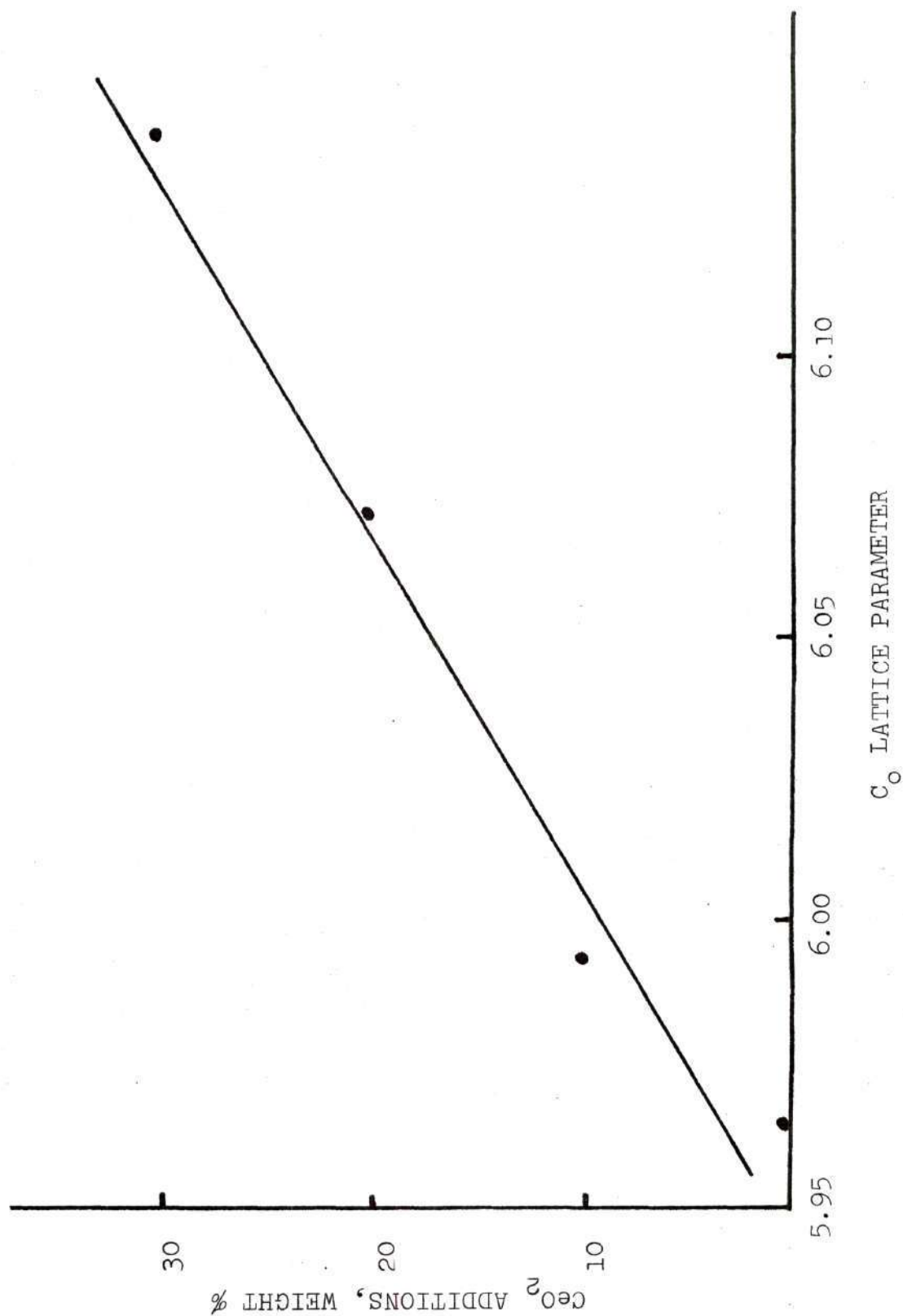


Figure 15. Increase in C_O Lattice Parameter of Nd₂O₃ (Calculated from (0002) Planes) as a Function of CeO₂ Additions.

double pass sample showed a very poor structure similar to those seen in the pure sesquioxides-metal systems (see Figure 16). During the first pass the CeO_2 is converted to Ce_2O_3 releasing oxygen which loosely combines with the metal in the liquid allowing it to go into solution. Upon solidification the metal returns to the metallic state and the oxygen is given off into the growth atmosphere. On the second pass the ceria was in the Ce_2O_3 state and did not contain enough oxygen to allow sufficient metal solubility to grow a uniform composite.

Metal Content and Growth Rate

Numerous trial and error experiments were conducted to determine the best starting metal composition. Figure 17 shows a sample grown at 2 cm/hr with a starting metal content of 15 wt% metal. The solidified zone consisted of metal dendrites in a matrix of eutectic material. When the starting metal content was reduced to 5 wt% metal the solidified zone consisted of oxide dendrites in a matrix of eutectic material as seen in Figure 18. Further investigation showed that only the coupled eutectic structure would solidify if a starting metal content of 10 wt% was used. This would indicate that the equilibrium eutectic mixture is about 10 wt% metal, however, the large amount of metal in blobs at the bottom of the solidified zone and in dendrites along the walls of the sample indicates that the true eutectic composition is much lower. Calculations of eutectic composition made from SEM photographs indicate that it is between 3 to 5 wt% metal.

When rare earth oxide-10 wt% Mo samples were solidified faster than 3.5 cm/hr, a disordered area of oxide dendrites in a matrix of

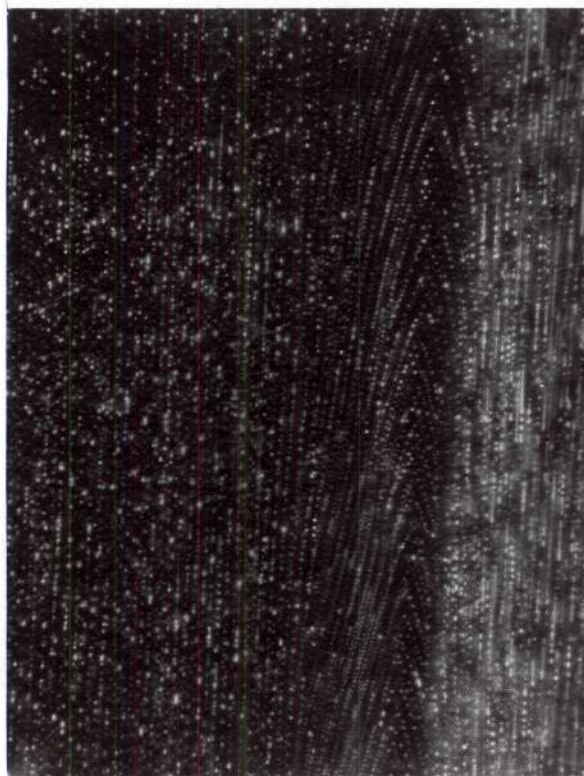


Figure 16. Transverse Microstructure of a Gd_2O_3 - CeO_2 -Mo Sample Through which the Molten Zone was Passed Twice. Dark Field, X600.



Figure 17. Longitudinal Section of a Gd_2O_3 - CeO_2 -Mo Sample with a High Starting Metal Content,³ (Note the Metal Dendrite). Dark Field, X600.

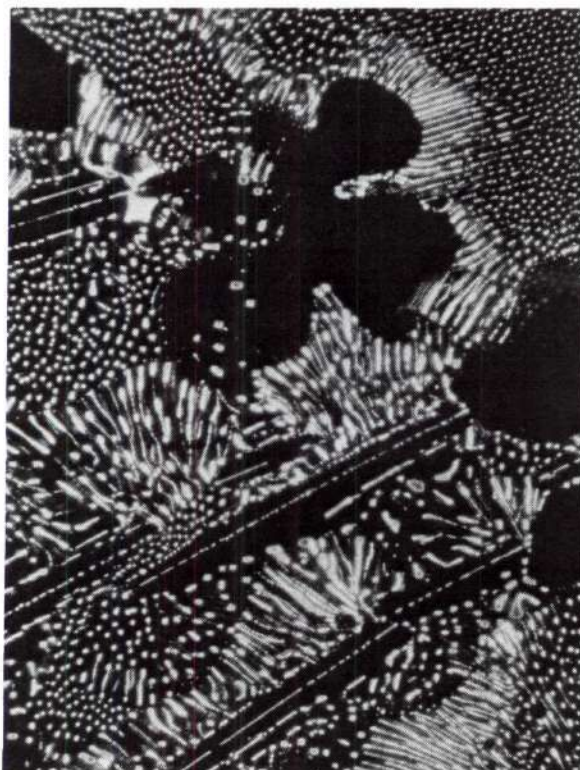


Figure 18. Transverse Section of a Gd₂O₃-CeO₂-Mo Sample with a Low Starting Metal Content, (Dark Areas are Oxide Dendrites). Dark Field, X600.

eutectic material appears along the longitudinal axis. This area is similar to the structure seen in metal deficient samples grown at slower rates. As the growth rate is increased this area increased in size until at 5 cm/hr it encompassed the entire solidified zone. At growth rates below 1 cm/hr numerous metal dendrites were seen in the solidified zone. These observations could be explained by the existence of a coupled region similar to that proposed by Hogan³⁶ and Tiller²³ for metal-metal systems. Hogan states that there is a range of compositions over which normal eutectic growth can be obtained if there is sufficient undercooling of the liquid. At zero growth rate, i.e., equilibrium, there is only one composition, the eutectic composition, which will produce coupled growth. However, if the growth rate is increased, thus increasing undercooling, a range of compositions can be solidified into normal composites. On a conventional phase diagram this region can be thought of as a metastable region spreading out from the eutectic below the solidus line. If the two phases have different melting temperatures, the coupled region will be skewed toward the higher melting phase. In the proposed pseudo-binary phase diagram is shown in Figure 19 and for a selected composition "A", as the growth rate (undercooling) is increased the structure will pass through three stages. First, at very slow rates, metal dendrites and eutectic regions will be observed; second, at moderate growth rates, the composition will be entirely in the coupled region and good composite growth will occur. Finally, as the growth rate is further increased, the composition will be outside of the coupled region requiring oxide dendrites to precipitate in the disordered region to

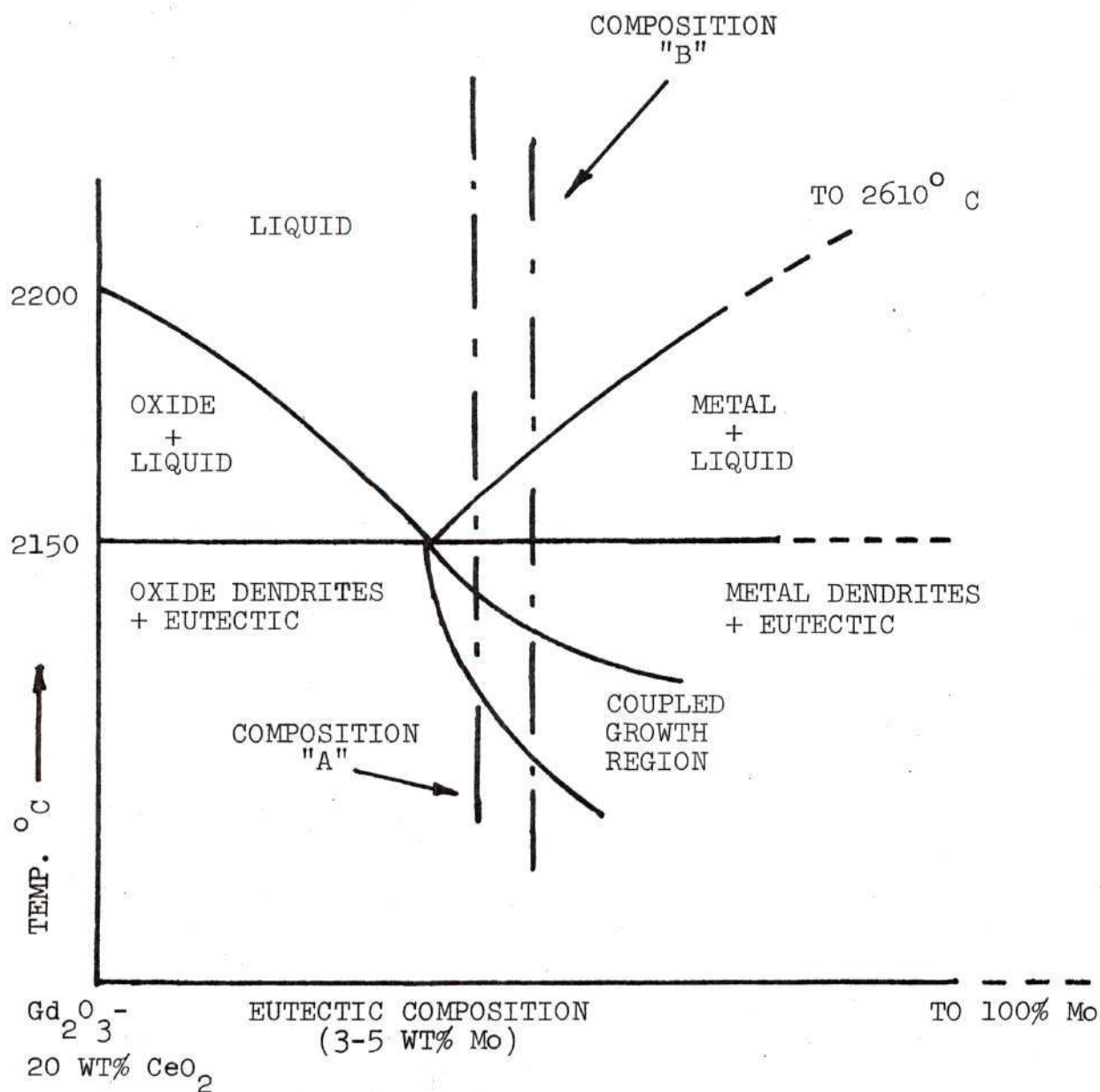


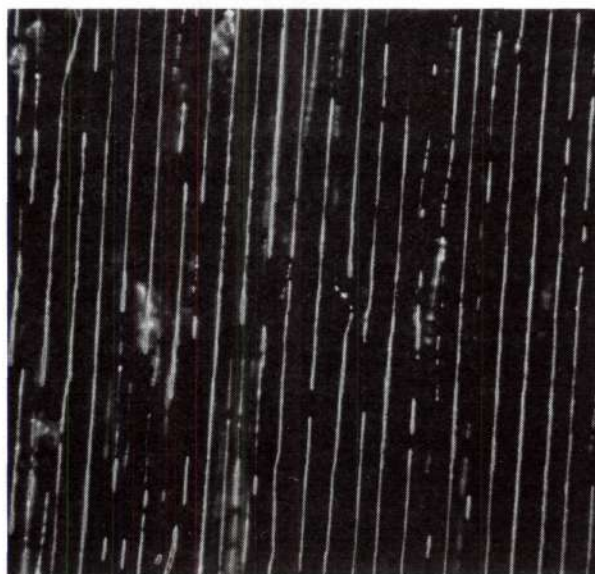
Figure 19. Proposed Pseudo-Binary Phase Diagram for the System Gd₂O₃-20 wt% CeO₂-Mo.

bring the composition back into the coupled zone. At even faster growth rates more primary oxide must precipitate in order to bring the composition into the coupled region and the disordered area increases in size until it encompasses the entire growth area. If, however, the original composition is moved to "B" (Figure 19), further toward the metal rich side, this composition will remain in the coupled zone at greater undercoolings without oxide precipitation. Table 2 summarizes experiments run at high growth rates with excess metal in an effort to experimentally observe this phenomenon. Although good results were obtained with one sample (Gd_2O_3 20 wt% CeO_2 -12 wt% Mo at 4.3 cm/hr), the existence and extent of a coupled zone is still inconclusive. It is felt that even though undercooling should be increased by increasing the growth rate, the difference could be so small as to make extremely rapid growth rates necessary to change undercoolings a significant amount. It is also probable that the growth kinetics, such as mixing and melting, cannot be successfully carried out at greatly increased growth rates. This conclusion is born out by the undissolved metal "blobs" seen in good composite areas while other areas in the sample are oxide rich. There is probably just not enough time to get the metal dissolved and distributed evenly across the growth front when samples are grown too rapidly.

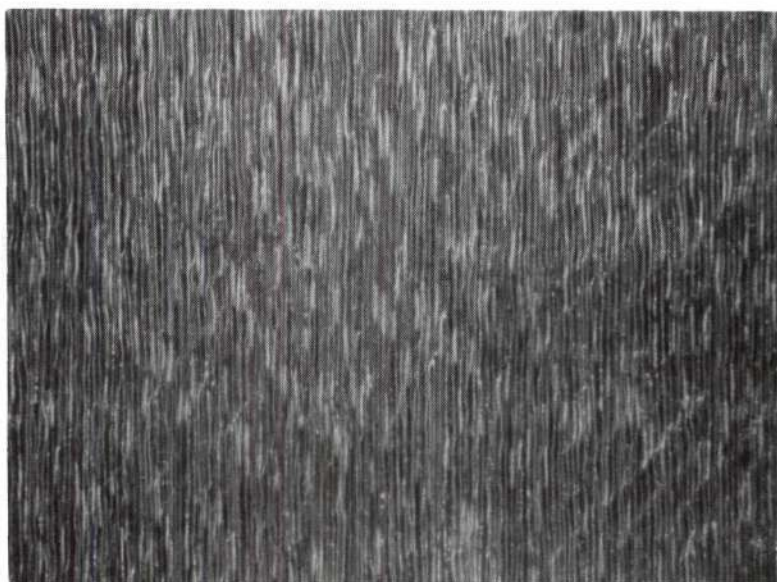
The most obvious effect of growth rate was to control the average fiber diameter and fiber density. Figure 20 shows longitudinal microstructures of good fiber areas in two Gd_2O_3 - CeO_2 -Mo samples grown at different rates, note the marked difference in fiber diameter and density. Fiber density measurements were calculated by counting the

Table 2. Summary of the Solidification of Excess Metal $\text{Gd}_2\text{O}_3(\text{CeO}_2)$ -Mo Samples Grown at Rapid Rates to Test the Coupled Growth Theory.

| Composition Weight % | Growth Rate Cm/Hr | Comments |
|---|----------------------|--|
| Gd_2O_3 20% CeO_2 12% Mo | 10 | Oxide Dendrites + Eutectic Very Little Excess Mo |
| Gd_2O_3 20% CeO_2 12% Mo | 6 | Oxide Dendrites + Eutectic Very Little Excess Mo |
| Gd_2O_3 15% CeO_2 15% Mo | 8.2 | Oxide Dendrites Some Fiber Areas Near Metal Blobs |
| Gd_2O_3 20% CeO_2 12% Mo | 4.3 | Good Uniform Growth |
| Gd_2O_3 20% CeO_2 14% Mo | 6.4 | Oxide Dendrites + Fiber Growth Near Metal Blobs |
| Gd_2O_3 20% CeO_2 12% Mo | 4.9 | Oxide Dendrites + Eutectic |



(a) Growth Rate 1 cm/hr



(b) Growth Rate 4 cm/hr

Figure 20. Typical $\text{Gd}_2\text{O}_3\text{-CeO}_2\text{-Mo}$ Samples Cut Parallel to the Growth Direction Showing the Effect of Different Growth Rates on Fiber Structure. Dark Field, X600.

number of fibers in a 9 cm^2 area of a 600X transverse micrograph and correcting for magnification. Figure 21 shows that fiber density increased in a near linear manner up to 5 cm/hr. Due to the small size of the fibers, SEM photographs were the only way to measure fiber diameters. Although not enough data was obtained to plot a graph of fiber diameter versus lowering rate; it was determined that fiber diameters vary about 25% around the average diameter, and the average fiber diameter is around 1.5 and $4.5 \times 10^{-5} \text{ cm}$ for growth rates of 4 and 1 cm/hr, respectively.

Metal Morphology

Ideally, these composites should have 100% rod shaped fibers in a regular array to produce the best electron field emitters. Although by far the most common metal morphology in the rare earth oxide-metal composites was rod shaped fibers, two other morphologies, platelets and rarely, at very slow growth rates, trifolils have been observed (see Figure 22). Since a 100% rod type fiber morphology was desired studies were made to determine when and why platelets occurred, in an attempt to eliminate them.

It was observed that platelets are more predominant at cell boundaries and tend to increase in size and number with increasing growth length. Figure 23 shows a Nd_2O_3 -20 wt% CeO_2 -10 wt% Mo sample transversely sectioned at intervals above the abse of the sample. Note the gradual change from a predominately rod type structure at the beginning of the unidirectionally solidified area to a predominately lamellar structure at the end of the solidified zone where the last liquid solidified. Slow growth rates also tend to favor platelet

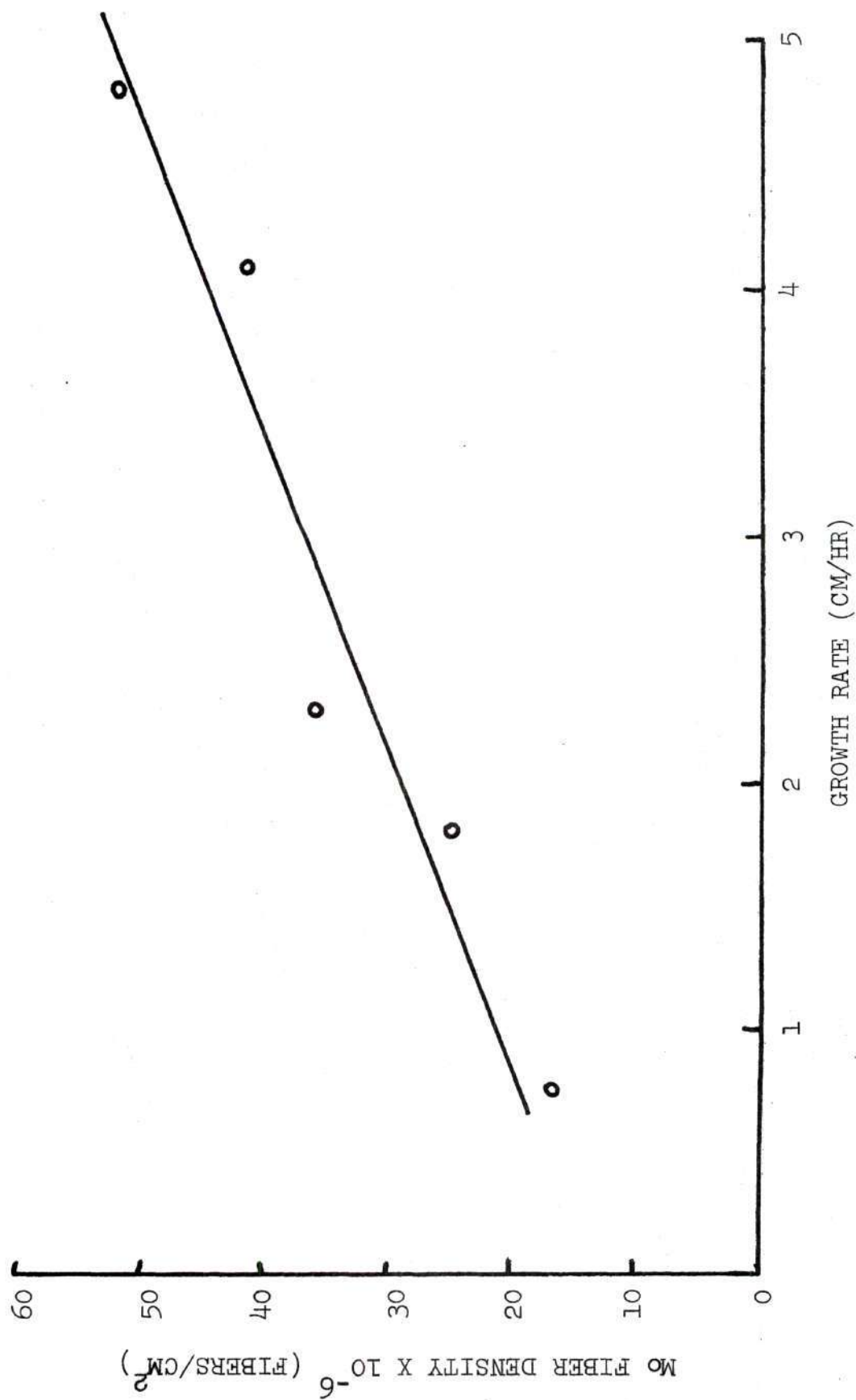
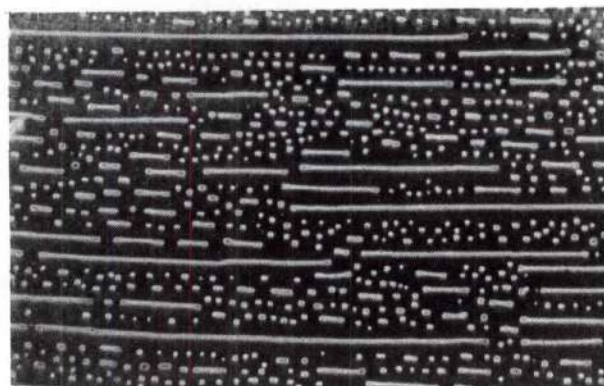


Figure 21. Effect of Growth Rate on Fiber Density in the System Gd_2O_3 -20 wt% CeO_2 -Mo.



(a) Mo Fiber or Rod Growth

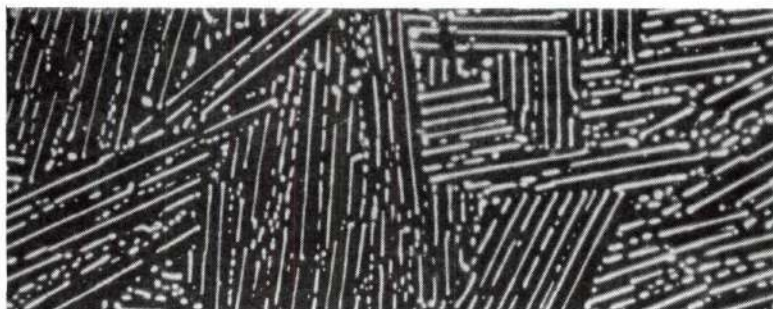


(b) Mo Platelet or Lamellar Growth

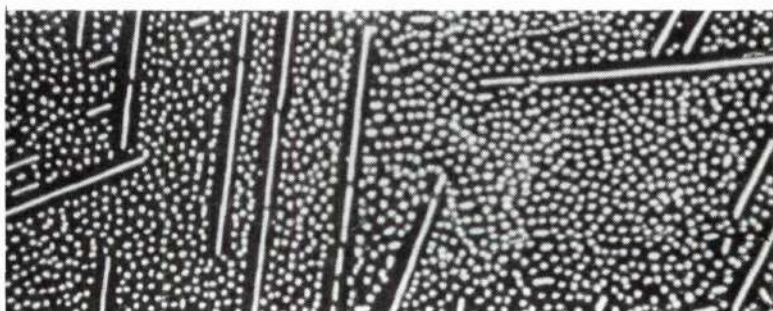


(c) Random Mo Trifoil Growth

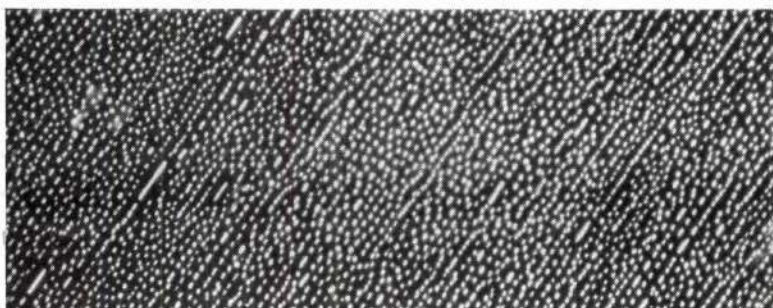
Figure 22. Transverse Sections of $\text{Nd}_2\text{O}_3\text{-CeO}_2\text{-Mo}$ Samples Displaying Three Types of Mo Morphology, Dark Field, X600.



(d) Last Liquid to Solidify 30 mm Above Base



(c) 24 mm Above Base



(b) 15 mm Above Base



(a) First Liquid to Solidify, Base

Figure 23. Transverse Sections of 20 wt% CeO_2 Doped Nd_2O_3 -Mo Sample Showing the Transition From Fiber to Platelet Morphology From Base to Top of the Solidified Zone. Dark Field, X600.

formation. Figure 24 shows a typical microstructure of a Gd_2O_3 -20 wt% CeO_2 -10 wt% Mo sample grown at 4 cm/hr. Platelets are only present at cell boundaries, and no cell contains only platelets. However, when the growth rate was reduced to 2 cm/hr (see Figure 25) some cells contained almost entirely platelets and most cells contained a few platelets in their interior.

The fact that platelets predominate in high impurity areas and are favored by slow growth rates has suggested a possible mechanism of rod to plate transformation. Due to the significant difference in the melting point of the two phases (2610°C for Mo versus 2200°C for Gd_2O_3), and the high volume ratio difference (at least 10 to 1 oxide to metal), it is reasonable to assume the metal phase leads the oxide phase at the solidification front. For pure materials this lead would be insignificant, but in the presence of impurities which would preferentially build up in front of the lagging oxide phase the metal lead distance would be increased.^{28,30} In the metal-metal systems where the volume ratios are typically low, and a lamellar structure predominates a lead by one phase will promote bridging causing the lagging phase to appear with a rod structure. In ceramic metal systems where the volume of the metal is low there is not sufficient metal to bridge the oxide phase, but the lead may give the metal time to grow in a secondary growth direction forming short platelets as shown in Figure 26. Although slow growth rates tend to decrease lead distance, this factor will be offset by the increase in time the secondary growth direction has to operate.

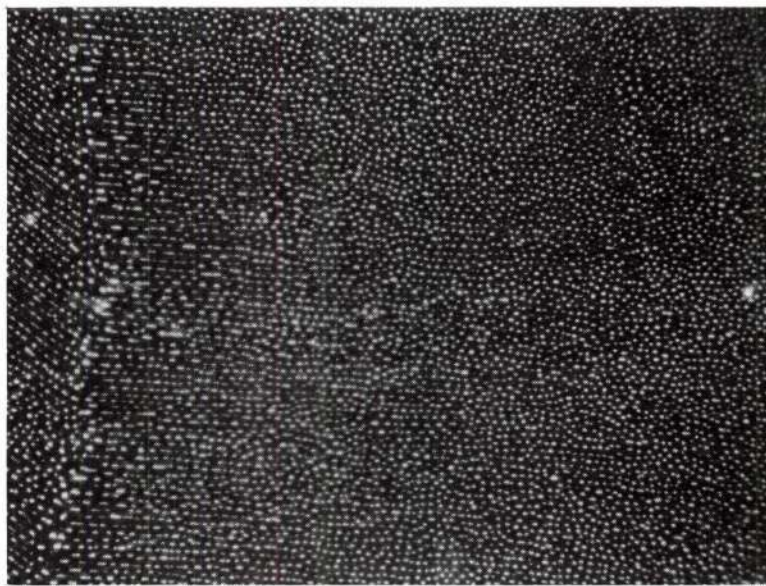


Figure 24. CeO_2 Doped Gd_2O_3 -Mo Sample Grown at 4 cm/hr Displaying Mo Fibers in the Cell Interior Which Gradually Change to Platelets as the Cell Boundary is Approached. Dark Field, X600.

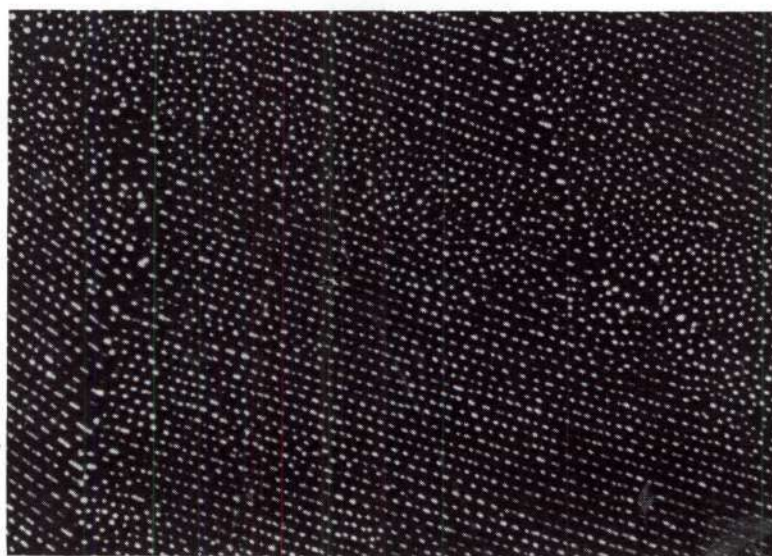


Figure 25. CeO_2 Doped Gd_2O_3 -Mo Sample Grown at 2 cm/hr Showing Cells Essentially Composed of Narrow Mo Platelets. Dark Field, X600.

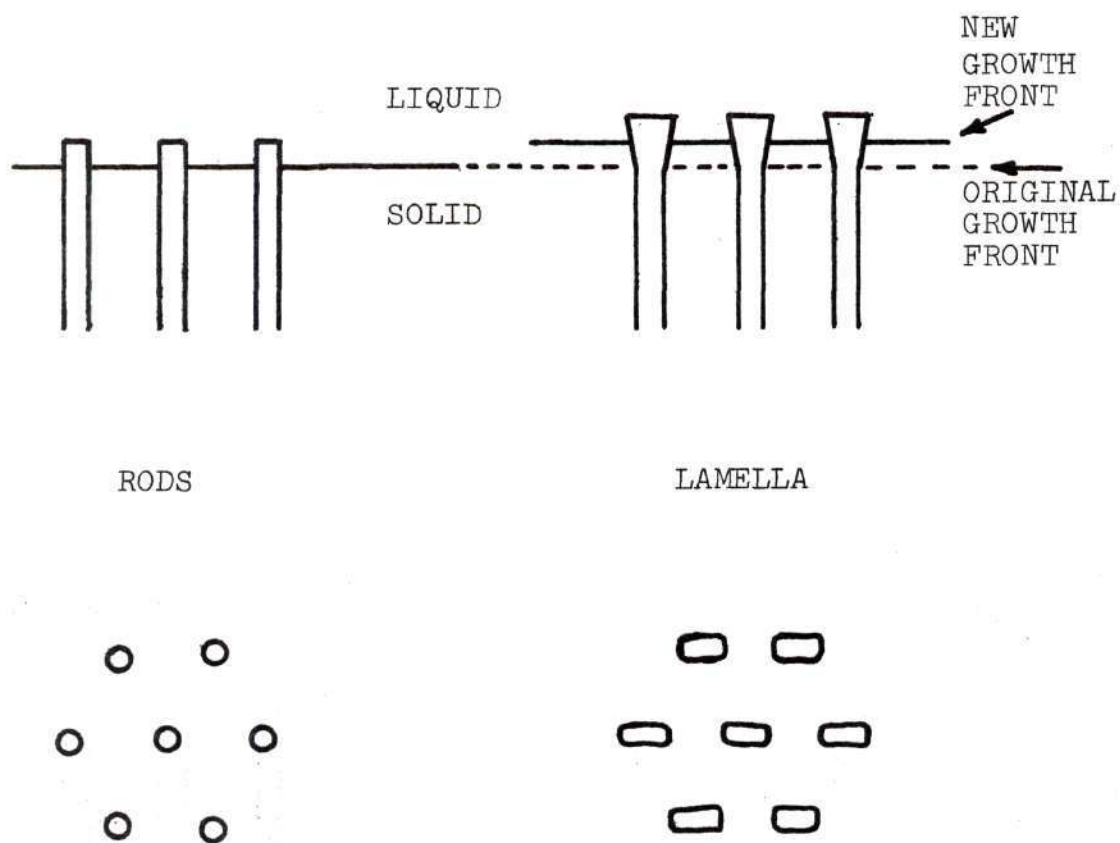


Figure 26. Schematic Diagram Showing how a Lead by the Metal Phase Over the Oxide Might Allow the Metal to Grow in a Secondary Direction and Form a Platelet or Broken Lamellar Structure.

Banding

Examination of unidirectionally solidified rare earth oxide-metal composites reveals two distinct types of metal fiber discontinuities (Banded growth). In the first type as seen in Figure 27 the fibers stop, and there is a band of oxide with disordered metal particles above which the fibers renucleate. In the second type of banded growth as shown in Figure 28, the fibers stop, are interrupted by a narrow band of pure oxide, and then continue directly aligned over the lower fibers. Of the many possible mechanisms that could cause banded growth, mechanical vibration, non-uniform lowering, and power fluctuations seemed the most likely. A series of samples were grown to determine which of these mechanisms caused banded growth. All samples were Nd_2O_3 -20 wt% CeO_2 -10 wt% Mo, the lowering rate was 2 cm/hr and the skin temperature and power settings were kept as constant as possible. The results of these experiments are presented in Table 3. They show that mechanical vibration and minor variation in lowering rate play little or no role in producing banded growth. The most significant finding was that power fluctuations, specifically power decreases caused the type of banding shown in Figure 27. Figure 29 shows a transverse section through the solidified zone of a composite sample that was subjected to the 2% power fluctuations noted in Table 3. The resultant regularly spaced bands are very distinct.

Note that in order to obtain repetitive power fluctuations and still maintain uniform growth conditions, the power must be first decreased before it is increased and conversely increased before it is decreased. However, it is felt that cycling the power resulted in

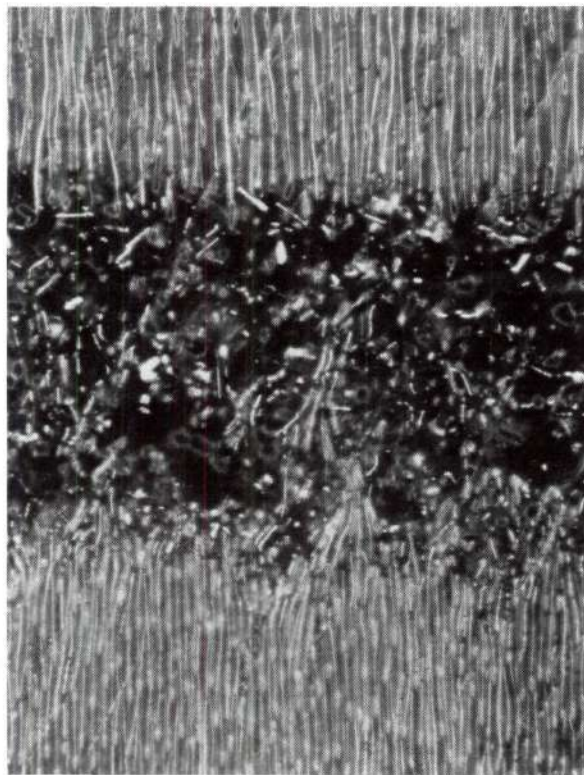


Figure 27. Longitudinal View of a Band of Oxide Containing Disordered Metal Particles. This is a Higher Magnification View of One of the Bands Induced Through Power Fluctuations in the Sample Shown in Figure 29. Dark Field, X600.

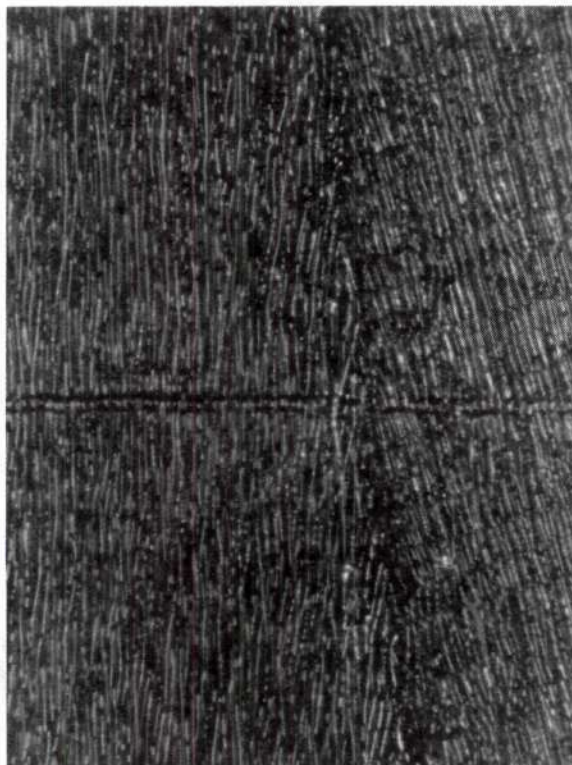


Figure 28. Longitudinal Section of a $\text{Nd}_2\text{O}_3\text{-CeO}_2\text{-Mo}$ Sample Showing Two Narrow Bands of Pure Oxide with Aligned Fibers Above, and Below the Discontinuity. Also Note the Typical Vertical Boundary. Dark Field, X600.

Table 3. Summary of Attempts to Artificially Induce Interrupted (Banded) Fiber Growth in $\text{Nd}_2\text{-O}_3\text{-CeO}_2\text{-Mo}$ Samples

| Treatment of Sample During Growth | Effect on Degree of Banding |
|--|---|
| Mechanical vibration of sample. | Possibly less banding than normal. |
| Stopping growth (sample lowering) for 10 seconds at 5 minute intervals. | Normal random bands. |
| Power increased 2% for 10 seconds, then returned (<u>decreased</u>) to normal, repeated at 5 minute intervals. | Regularly spaced bands at distances corresponding to 5 minutes of zone travel. Sample shown in Figures 27 and 29. |
| Power decreased 2% for 10 seconds, then returned (<u>increased</u>) to normal, repeated at 5 minute intervals. | Normal random bands. |
| Random increases and decreases of power for various durations of time. | Only power increases for longer than 1 second followed by power <u>decreases</u> appear to reduce bands. |

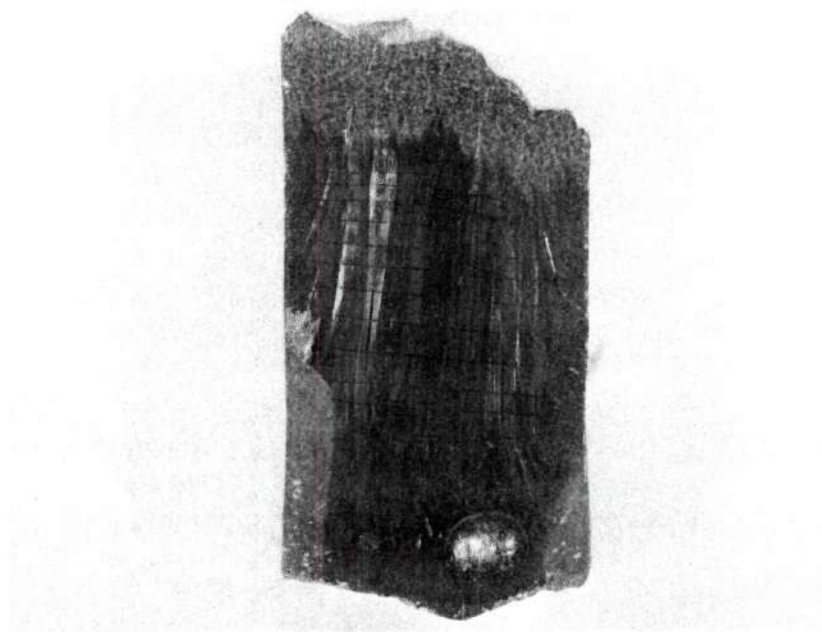


Figure 29. Longitudinally Sectioned Molten Zone of a $\text{Nd}_2\text{O}_3\text{-CeO}_2\text{-Mo}$ Sample Showing Regularly Spaced Bands Induced Through Periodic Power Fluctuations. X2.0.

the same behavior as would be obtained for a simple power decrease or increase. In the case of the samples subjected to an initial power decrease there would be negligible sample growth during this fluctuation since the band of disordered growth will be remelted by the subsequent power increase and composite growth will appear continuous. In the case of the initially increased samples the increase will remelt some of the already solidified composite and once the power is subsequently reduced it will resolidify this as a disordered band. It should also be noted that 2% fluctuations were used because line voltage fluctuations of that magnitude are often seen.

The reason power fluctuations caused banding can be explained by the fact that the size of the molten zone was controlled by the amount of available power, and apparently the size of the molten zone changed very rapidly with small changes in input power. During growth when the power increased abruptly some of the already solidified composite remelted. After equilibrium growth was reestablished at the normal power settings, the oxide-metal solidification resumed without any major disruption of the composite structure. However, when the power was suddenly decreased, a layer of oxide and metal was solidified much too rapidly to produce ordered growth, and the oxide band containing the Mo particles resulted. Then as controlled solidification started again the fibers renucleated, and ordered composite growth proceeded.

It is interesting to note that none of the attempts at artificially inducing banding produced the second (narrow oxide) type of band described earlier. At this time there is no satisfactory explanation of how this type of band arises.

Chemical Etching

One of the main reasons oxide-metal composites were investigated was their possible use as efficient electron field effect emitters. For this application many composite geometries were required, including the removal of the fibers to leave holes, and the selective removal of the oxide matrix to form arrays of fibers with both blunt as well as pointed fiber tips. A series of chemical etching experiments were done in conjunction with the growth work and they are important enough to be included in this paper. However, the etching and electronic theory are outside the scope of this paper and will not be recounted, instead the reader is referred to reference 9 and J. Peppers masters thesis⁴⁵.

All etching work was done on Gd_2O_3 -20 wt% CeO_2 -10% wt% Mo samples which were grown in as nearly the same manner as possible and cut into wafers perpendicular to the fiber growth direction. The wafers were polished, and etched while rotating at about 10 RPM at room temperature, in the etching rig described by Pepper.⁴⁵ It was discovered that a mixture of 75 g of potassium ferrocyanide and 20 g of sodium hydroxide dissolved in 250 ml of water would selectively etch the Mo metal without disturbing the matrix as seen in Figure 30.

When selectively etching the matrix to expose blunt and pointed fibers it was found that annealing was beneficial to heal microcracks introduced by the high thermal gradient inherent in the zone melting technique. Annealing was accomplished by heating the specimens to 1800°C in an H_2-N_2 atmosphere using the rf generator and a moly suceptor much the same way samples are preheated prior to internal

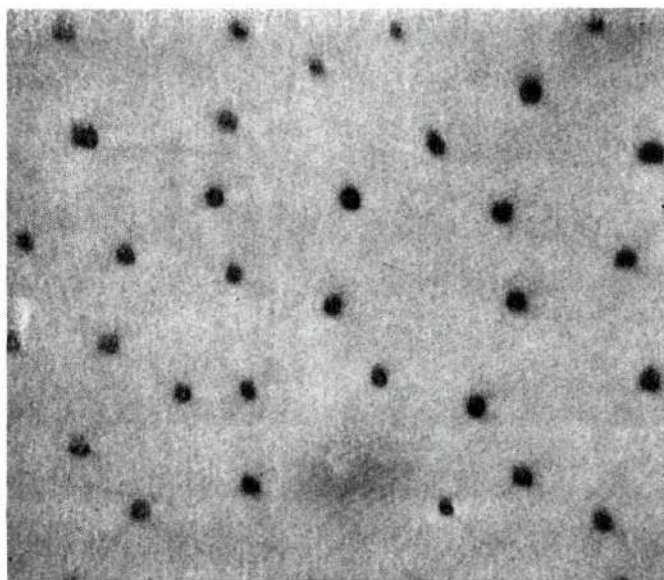
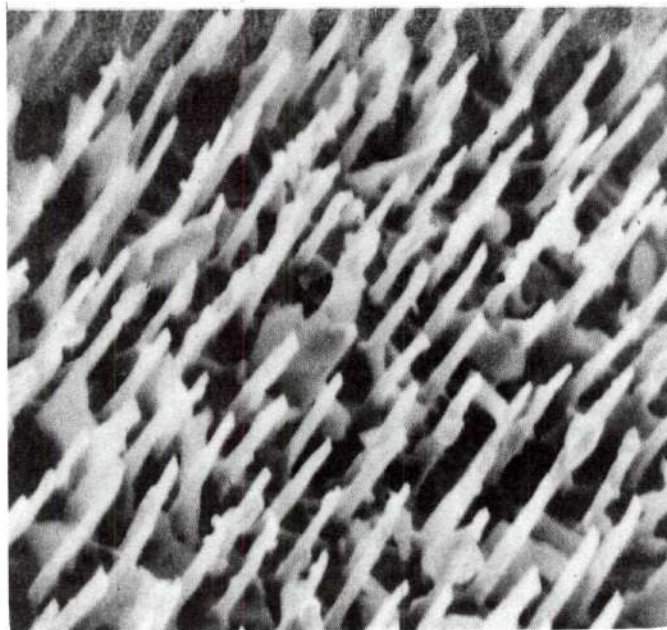


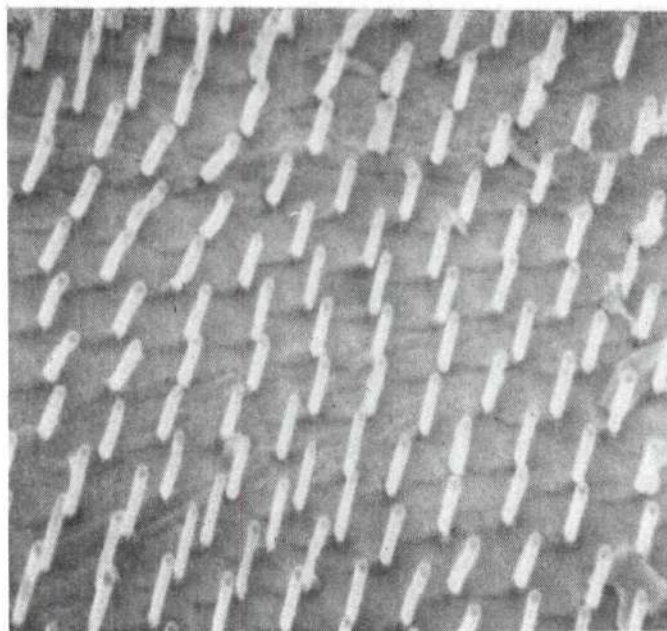
Figure 30. Scanning Electron Micrograph Showing the Selective Etching of the Mo Fibers Leaving an Array of Holes in the Oxide Matrix. X9,000.

melting. The samples were then slow cooled to room temperature in about 2 hours. Figure 31 shows the difference in matrix roughening during etching of an annealed and unannealed specimen etched in the same manner.

Once matrix roughness was found to be due to microcracks rather than the etchant, it was soon discovered that concentrated sulfuric acid attacked the matrix without roughening it and without damaging the fibers. The samples shown in Figure 31 were both etched with sulfuric acid. Note the blunt fiber tips and smooth matrix in the annealed specimen. Additions of a small amount of ammonium nitrate to the sulfuric acid etch caused the fibers to be attacked as well as the matrix, but at a different rate, producing pointed tips as seen in Figure 32. Further investigation into the pointing composition showed that as the ammonium nitrate concentration was increased from 1/2 to 1-1/2 g per 50 ml of concentrated sulfuric acid the fibers were pointed but were shorter as seen in Figure 32. Also the minimum etching time needed to produce fully pointed tips decreased from ten to six minutes. The smoothest matrix and the most uniform fiber pointing was obtained by etching for eight minutes in a solution of 1 g ammonium nitrate in 50 ml concentrated sulfuric acid. A more detailed investigation of the etching behavior of $\text{Gd}_2\text{O}_3\text{-CeO}_2\text{-Mo}$ was undertaken from this point by Rieger.⁴⁶

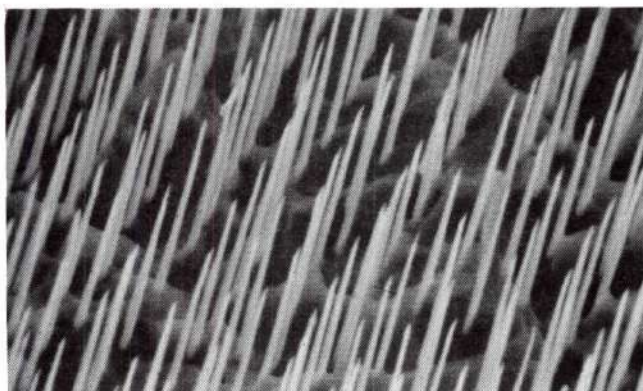


(a) Unannealed.

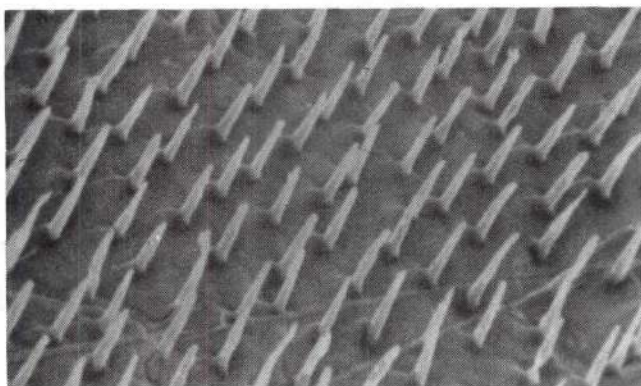


(b) Annealed.

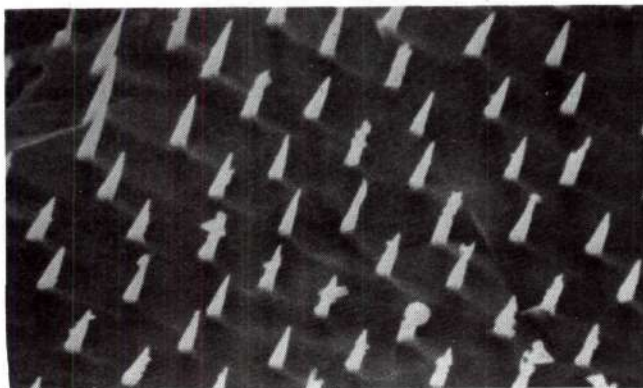
Figure 31. SEM Photographs Showing the Striking Improvement in Etching Uniformity Resulting from Annealing Prior to Etching. X5,000.



(a) $1/2$ g NH_4NO_3 / 50 ml H_2SO_4 .



(b) 1 g NH_4NO_3 / 50 ml H_2SO_4 .



(c) $1-1/2$ g NH_4NO_3 / 50 ml H_2SO_4 .

Figure 32. SEM Photographs of a Series of Samples Etched with NH_4NO_3 in Sulfuric Acid to Determine the Effect of Increasing NH_4NO_3 Content. X5,000.

CHAPTER VI

CONCLUSIONS

1. The internal molten zone technique can be used to unidirectionally solidify a variety of rare earth oxide-metal compositions.
2. The lanthana and neodymia metal systems when unidirectionally solidified showed poorly aligned non-uniform eutectic growth due to poor metal solubility in the molten oxide.
3. The addition of CeO_2 (optimally 20 wt%) dramatically improved eutectic structure in the sesquioxide-metal systems by retaining oxygen in the sample until melting occurred thus increasing metal solubility in the molten oxide.
4. Fiber diameter decreased and fiber density increased with increasing growth rate in the CeO_2 doped sesquioxide systems.
5. Fiber morphology was found to change from a primarily rod type morphology to a plate morphology as growth rate decreased and impurity levels increased.
6. One type of banding was proven to be due to minor power fluctuations during growth.
7. Various etching techniques were developed in order to produce various fiber-matrix geometries of interest for use in electron field effect emitter testing.

BIBLIOGRAPHY

1. Tudbury, C. A., Basics of Induction Heating, Volume I, John F. Ryder Publisher, Inc., 1960.
2. Leatherman, A. F., and Stutz, D. E., "Induction Heating Advances: Application to 5800°F.", Office of Technology Utilization, National Aeronautics and Space Administration, Washington, D. C., 1969.
3. Viechnicki, D., and Schmid, F., "Eutectic Solidification in the System $\text{Al}_2\text{O}_3/\text{Y}_3\text{Al}_5\text{O}_{12}$," Journal of Material Science, Volume 4, pp. 84-88, 1969.
4. Haggerty, J. S., Lee, D. W. and Wenckus, J. F., "Preparation and Characterization of High Quality Single Crystal Refractory Metal Borides and Carbides," Technical Report AFML-TR-68-228, Air Force Materials Lab, pp. 19-20, December 1968.
5. Holt, J., "Refining and Growth of Rutile Single Crystals by R. F. Zone Melting," British Journal of Applied Physics, Volume 16, pp. 634-41, 1965.
6. Nestor, O. H., "Symmetrical Laser Crystals," Final Technical Report, Contract Nonr-4131(00), Program Code no. 3730 ARPA Order 306-62, Task No. NR017-708, Union Carbide, November, 1965.
7. Chapman, A. T. and Clark, G. W., "Growth of UO_2 Single Crystals Using the Floating-Zone Technique," Journal of the American Ceramic Society, 48, pp. 493-95, September, 1965.
8. Hill, D. N., "Internal Zone Melting of Refractory Oxides Using Induced Eddy-Current Heating," M.S. Thesis, Georgia Institute of Technology, 1969.
9. Hill, D. N., "Internal Zone Melting of Refractory Oxides Using Induced Eddy Current Heating," Masters Thesis in the School of Ceramic Engineering Georgia Institute of Technology, 1969.
10. Chapman, A. T., Clark, G. W. and Hendrix, D. E., " UO_2 -W Cermets Produced by Unidirectional Solidification," Journal of the American Ceramic Society, Volume 53, p. 60, 1970.
11. Chapman, A. T., et al., "Unidirectional Solidification Behavior in Refractory Oxide-Metal Systems," Journal of Crystal Growth, Volume 13/14 pp. 765-71, 1972.

12. Jen, C., "Factors Determining the Unidirectional Solidification Behavior of the Systems UO_2 -Ta, UO_2 -Nb, and UO_2 -Mo," Masters Thesis in the School of Ceramic Engineering, Georgia Institute of Technology, 1972.
13. Watson, M. D., Hill, D. N., and Chapman, A. T., "Solidification Behavior of Stabilized ZrO_2 -W," Journal of the American Ceramic Society, Vol. 53, p. 112, 1970.
14. Watson, M. D., Johnson, T. A., Benzel, J. F. and Chapman, A. T., "Unidirectional Solidification of Tungsten in Stabilized ZrO_2 and HfO_2 ," Proceedings of the Conference on In Situ Composites, Lakeville, Connecticut, p. 157, September 5-8, 1972.
15. Watson, M. D., "Stabilized ZrO_2 -W Composites Produced by Unidirectional Solidification," Masters Thesis in the School of Ceramic Engineering, Georgia Institute of Technology, 1973.
16. Johnson, T. A., "Unidirectional Solidification of Tungsten in Stabilized Hafnia," Masters Thesis in the School of Ceramic Engineering, Georgia Institute of Technology, 1972.
17. Nelson, R. P. and Rasmussen, J. J., "Composite Solidification in the Systems Cr_2O_3 -Mo, Cr_2O_3 -W, and MgO -W," Journal of the American Ceramic Society, Volume 53, p. 527, 1970.
18. Hart, P. E., "New Class of Ceramic Composites," Ceramic Age, Volume 88, Number 3, pp. 29-30, 1972.
19. Latta, R. E., Fryxell, R. E., "Determination of Solidus-Liquidus Temperatures in UO_2 -X Systems (-0.5×0.20)," Journal of Nuclear Materials, Volume 35, pp. 195-210, 1970.
20. Sundquist, B. E., and Mondolfo, L. F., "Heterogeneous Nucleation in the Liquid to Solid Transformation in Alloys," Transactions of the Metallurgical Society of AIME, Volume 221, pp. 157-64, February, 1961.
21. Sundquist, B. E., and Mondolfo, L. F., "Orientation Relationships in the Heterogeneous Nucleation of Solid Lead from Liquid Lead," Transactions of the Metallurgical Society of AIME, Volume 221, pp. 607-613, June 1961.
22. Wiengard, W. C., "Fundamentals of the Solidification of Metals," Metallurgical Reviews, Volume 6, No. 21, 1961.
23. Tiller, "Polyphase Solidification," Liquid Metals and Solidifications, ASM, p. 278, Cleveland, 1958.

24. Chadwich, G. A., "Eutectic Alloy Solidification," Progress in Materials Science, Volume 12, Number 2, p. 113, 1963.
25. Mollard, F. R., and Flemings, M. C., "Growth of Composites from the Melt," Office of Naval Research Technical Report, Number 2, November, 1966.
26. Schiel, E., "Über die eutektische Kristallisation," Zeitschrift Metallkunde, Volume 45, p. 298, 1954.
27. Jackson, K. A., and Hunt, J. D., "Lamellar and Rod Eutectic Growth," Transactions of the Metallurgical Society of AIME, Volume 236, pp. 1129-42, August, 1966.
28. Chadwich, G. A., Metallography of Phase Transformations, Butterworths London, 1972.
29. Lemkey, F. D., et al., "The Microstructure, Crystallography and Mechanical Behavior of Unidirectionally Solidified Al-Al₃Ni Eutectic," Transactions of the Metallurgical Society of AIME, Volume 233, pp. 334-41, 1965.
30. Cooksey, et al., "The Control of Eutectic Microstructures," Journal of the Australian Institute of Metals, Volume 5, Number 3, p. 34, 1960.
31. Hunt, J. D., and Chilton, J. P., "Rod-Plate Transition", Journal Institute of Metals, Volume 92, p. 21, 1963.
32. Chalmers, B., Principles of Solidification, Wiley, New York, 1964.
33. Hunt, J. D., and Jackson, K. A., "Binary Eutectic Solidification," Transactions of the Metallurgical Society of AIME, Volume 236, pp. 834-843-67, June, 1967.
34. Chadwich, G. A., "Solidification of CuAl₂-Al Eutectic Alloys," Journal of the Institute of Metals, Volume 91, pp. 169-73, 1963.
35. Keneko, J., Flemings, M. C., "Effects of Turbulent Convection on the Structures of Unidirectionally Grown Al-CuAl₂ Eutectics," Chapter 2, Technical Report #3, Office of Naval Research Contract NONR-3963(09), 1969.
36. Hogan, L. M., "The Solidification of Binary Eutectic Alloys," Journal of the Australian Institute of Metals, Volume 6, Number 4, p. 279, 1961.
37. Johnson, W. C., et al., "Separation of the Rare Earth Elements by Ion Exchange," Chemical Engineering News, Volume 25, p. 2495, 1947.

38. Yao, R. A., "Substoichiometric Rare-Earth Oxide Compounds," Journal Inorganic Nuclear Chemistry, Volume 22, pp. 1483-87, 1965.
39. Brauer, G., "Structural and Solid State Chemistry of Pure Rare Earth Oxides," Progress in the Science and Technology of the Rare Earths, Pergamon Press, Oxford England, 1964.
40. Ploetz, G. L., Krystyniak, C. W., and Dumes, H. E., "Sintering Characteristics of Rare-Earth Oxides," Journal of the American Ceramic Society, pp. 551-4, Volume 41, 1958.
41. Curtis, C. E., and Johnson, J. R., "Ceramic Properties of Samarium Oxide and Gadolinium Oxide; X-Ray Studies of Other Rare-Earth Oxides and Some Compounds," Journal of the American Ceramic Society, Volume 40, 1957.
42. Bevin, D. J. M., and Kordis, J., "Mixed Oxides of the Type MO_2 (Fluorite)- M_2O_3 -I Oxygen Dissociation Pressures and Phase Relationships in the System CeO_2 - Ce_2O_3 at High Temperatures," Journal of Inorganic Nuclear Chemistry, Volume 26, pp. 1509-23, 1964.
43. Mozzi, R. L., Guentert, O. J., "X-Ray Study of Phase Transformations in Some Rare-Earth Oxide Systems," The Journal of Chemical Physics, Volume 36, pp. 298-301, 1961.
44. Burke, M. A., " CeO_2 -Mo Composites Produced by Unidirectional Solidification" Masters Thesis in the School of Ceramic Engineering Georgia Institute of Technology, 1974.
45. Pepper, J., "The Etching Behavior of Uranium Dioxide-Tungsten Composites," Masters Thesis in the School of Ceramic Engineering, Georgia Institute of Technology, 1970.
46. Rieger, A. R., "The Selective Chemical Etching of CeO_2 Doped Gd_2O_3 -Mo Composites," Masters Thesis in the School of Ceramic Engineering, Georgia Institute of Technology, 1973.